SUPERADONE

design study

INFN

march 1974

LNF

4 - EXPERIMENTS WITH SUPERADONE

C. Mencuccini, P. Spillantini, I. Peruzzi, M. Piccolo, F. Ronga, L. Paoluzzi, G. Barbiellini, G. Vignola, B. Stella, R. Santangelo, R. Biancastelli.

4.1 - Introduction

The aim of Chapter 4 is to discuss the general aspects of the experimentation around a high energy e^+e^- storage ring and to foresee, in due time, possible crucial interference regions between users and machine builders. In this limited frame only general lines will be explored and no particular experiment will be considered: the physics which can be anticipated on the basis of the present knowledge will anyway provide the necessary framework in order to outline the general trends for a correct "first approach" experimental programme.

The main working hypotheses, on which the present analysis is based, are that a total c.m. energy of 20 - 25 GeV and a luminosity of $10^{32} cm^{-2} s^{-1}$ will be achieved and that 2 (and possibly 4) 6 m long straight sections will be available for the experimentation. The situation of some typical counting rates is sketched in the general introduction (ch. 2) and the family of the accessible processes is also given.

Here, these e^+e^- induced processes will be divided into two main classes according to the minimum number of virtual photons involved: a first group refers to the usual annihilation processes via 1 photon exchange whose relevant experimental feature is that the total available c.m. energy is entirely released to the final products in a 1^- state; the reactions of the second class proceed through two-photon interactions and originate final states in which an electron and a positron are still present and forward emitted with respect to the beam line. The reasons for this distinction are connected with the different experimental

problems which rise when specific detectors are to be designed in the two cases.

In the following of sect. 4.1, a general survey of the experimental problems foreseen in order to fully exploit the potentialities of a SuperAdone type machine, will be given. More specific details and possible technical solutions will be discussed in section 4.2, 4.3 and 4.4. About the physical motivations supporting a certain number of technical attitudes, ch. 2 will be referred to.

Annihilation processes via the one-photon channel.

a) Two-body final states.

The most common Q.E.D. dominated processes, that is $e^+e^- \to e^+e^-$, $e^+e^- \to \gamma\gamma$, $e^+e^- \to \mu^+\mu^-$ give relatively high counting rates (order of several counts/minute) and their very peculiar experimental features make their detection easy and reasonably free from any background from competing processes. Obviously, serious experimental difficulties rise when absolute measureme with accuracies of the order of 1% are to be done. But, in thi case, these problems are not very different, in principle, from ones met at lower energies (absolute monitoring, detectio efficiencies, etc.) so that no particular consideration will be given them in this report.

Another very important class of possible two-body processes in the field of QED consists in the production (if any) of stable or quasi-stable point-like, colinear objects such as heavy leptons, constituents and so on. Should this kind of particles exist, the colinearity of the particles in the fina state and the typical threshold-like behaviour of the corresp ding couting rates as a function of the energy, would give a

very clear signature to the process. A third family of two-body processes is connected to the hadron form factors in the time-like region ($e^+e^- \to \pi^+\pi^-$, K^+K^-, $p\bar{p}$, ...). The expected counting rates are extremely small in this case and completely hopeless from the point of view of a systematic detection unless high mass vector mesons strongly coupled to the photons give spectacular enhancements at SuperAdone energies.

Therefore, apart from the $e^+e^- \to e^+e^-, \gamma\gamma$, $\mu^+\mu^-$ processes, the problem of the experimental investigation of the two-stable-body colinear events shoud be approached, in the light of the present knowledge, with a first generation simple and fast apparatus whose main features shoud be a reasonably high solid angle and a very good spacial sensitivity (in order to minimize the ambiguities in the colinear-like behaviour assignement to the events). As far as the nature of the detected particles is concerned, at least a rough distinction between high energy (machine energy) electrons and muons and any other particle is requested in order to depress the $e^+e^- \to e^+e^-$, $\mu^+\mu^-$ background signal, above which a threshold-type raise should appear once the machine energy reaches the value of the mass of the produced stable particle. The results obtained with such a two-body survey will clearly guide the design of the possible second approach apparata.

b) e^+e^- annihilation into many hadrons.

The most relevant features of the annihilation processes into many pions and kaons can be rather safely stated in the following points:

- the counting rates are relatively high: the presently conceivable cross sections are of the order of 10 nb and give events at rates of the order of a few thousands useful triggers per day;
- the average total multiplicities $< n >$ may be reasonably estimated in the range 8 - 10 with the further qualitative condition $< n_{\pi^0} > \simeq < n_{\pi^+} > \simeq < n_{\pi^-} >$. The multiplicity distribution around these average values may be reasonably assumed to be represented by a poissonian law according to which the dominant channels at each energy are pretty well concentrated around the corresponding average multiplicity, whereas processes involving lower or higher multiplicities are rather soon depressed and easily escape a systematic detection with the presently conceived luminosities. This fact in particular implies that the average energy per produced particle in the dominant detected channels may be considered as a not too much varying quantity as a function of the total c.m. energy made available by Super-Adone;
- the angular distribution of the produced particles should not show any preferred angular region and, in order to design detectors, a work hypothesis of isotropic distribution sounds reasonable and consistent with the conditions that the c.m. of the system is steady and the total available energy is entirely released to the produced particles. The momentum distribution of the produced pions assuming an invariant phase space is shown in fig. 4.2.33 in the case of 8 pions produced at 20 GeV total c.m. energy.

Facing the above mentioned general features of the onephoton annihilation reactions into many hadrons, one has to outline the main objectives of the experimental research in order to be able to specify the basic requirements for the experimental arrangements. A list of the physical subjects to be investigated has been already discussed in this report and may be summarized in the following points:

- total production cross section as a function of the energy;
- average multiplicities, charged and neutral, as a function of the energy;
- inclusive reactions on pions, kaons, unstable mesons, antiprotons, etc.;
- momentum correlations among groups of particles (jets, clusters, resonances, etc.);
- exclusive reactions at least for dominant channels, etc.

It is worth observing that the low multiplicity region (for instance the two charged non colinear configurations) might be fed by a mechanism of production of short life unstable point like pairs generating detectable decay products (e, μ , hadrons). It is clear that, in this case, the correct nature assignement to the particles and a great care in the beam-residual gas background subtraction are essential conditions in order to let these two-body production processes show up (if they exist).

All the above mentioned elements lead to a series of experimental requirements to be fullfilled by any suitable detector. The first of these requirements deals with the solid angles covered by the set-up, namely the solid angle where the charged particles can be detected, the solid angle where the momentum of the charged particles can be measured (in general smaller than the previous one) and the solid angle where the photons form π^0's (or η's) decay can be detected. The need for the detection of as many complete kinematical configurations as possible clearly leads to typical requirements of solid angles of the order of 80-90% of the total 4π sterad. By reaching such high solid angles the detection efficiencies for complete configurations of events of a certain produced multiplicity are

high enough to make reasonably easy the evaluation of the contamination to the detected channel from the reactions produced with higher multiplicity but appearing in the detector with the same topological configuration. Therefore, it is easy to show that, in order to get model indipendent detection efficiencies, solid angles of the order of 80-90% of 4π are needed, where charged particles and photons as well have to be detected. In this same respect, the further requirements of a good momentum analysis of at least part of the detected charged particles and of a less precise energy measurement of some of the detected photons will provide, beside other obvious advantages, the possibility of complementing the information got with the pure geometric detection.

Thus, within the mentioned solid angles, the main experimental requirements for a detector properly suited to study the many hadrons production in a SuperAdone type of storage ring, may be summarized in the following items:

- measurement of the emission angles of the detected charged particles;
- measurement of the emission angles of the detected photons;
- measurement of the momenta of the charged particles;
- measurement of the energy of the photons;
- recognition of the nature of the charged particles.

It is clear that all these requirements are in a way conflicting if one wants to fulfill them simultaneously. For instance a good momentum resolution (of the order of $\Delta p/p \simeq 1\%$ at 1 GeV/c) cannot easily be obtained over a large solid angle so that a choice has to be made between the two extreme attitudes of a poor resolution ($\Delta p/p \sim 3 \div 10\%$ up to $p \sim 5$ GeV/c) over a

large solid angle ($\Delta\Omega/4\pi \sim 80\%$) or of a good resolution but in a smaller solid angle ($\Delta\Omega/4\pi \sim 30$-$40\%$). By poor momentum resolution it has to be anyway intended a resolution such as to allow, for instance, the recognition of nucleon pairs in the final state or the clean reconstruction of ϱ masses from the momenta of pairs of pions. The line of a rather poor momentum resolution over a large solid angle seems to be more promising and flexible for the presently conceivable researches so that it will constitute a sort of guiding criterion in commenting the various experimental solutions discussed in the following sections. In this frame the π/K separation through complete kinematical reconstruction of the events is obviously very difficult and particular detectors will have to be inserted in the detection chain in order to achieve this separation. Therefore subsection 4.2.4 will concentrate on this point and a discussion about velocity selectors (Cerenkov counters) will be presented. The main conclusion will be that a π/K separation over the whole momentum range is resaonably feasible only in a rather limited angular region ($\Delta\Omega_{\pi/K}/4\pi \leq 20\%$) whereas for momenta below 2 GeV/c this discrimination will be possible over much larger solid angles.

c) Quasi real photon-photon interactions.

The physical aspects of the two photon processes $e^+e^- \to e^+e^-X$ have been previously discussed and relatively high counting rates are expected. Many of the considerations about the experimental arrangements discussed in connection with the e^+e^- annihilation into two or many hadrons, properly hold also in the case of the photon-photon interactions. But, in this case, some peculiar experimental feature is present which can be used in order to make easier the identification

of the process. The most relevant physical peculiarities of th photon-photon processes may be summarized in the following topics:

a) the incoming e^+ and e^- survive in the final state and are forward emitted within a very narrow cone around the beam line;

b) the center of mass of the wide angle emitted particles in general is not at rest and moves in a direction which is very close to beam line;

c) only a fraction of the available incident energy is released to the wide angle emitted particles system (both in the "resonance" or in the "diffraction dominated" region).

The experimental implications in order to evidentiate these features will be discussed in sect 4.3.

4.2. - MAGNETIC DEVICES AND DETECTION PROBLEMS

4.2.1. - Magnetic devices survey

The aim of this section is to briefly review the present situation as fa as large solid angle magnetic devices are concerned in view of the many hadron production processes detection. In this perspective, already built or designed devices will be recalled and the related references given, whereas their possible extensions at higher energies or newly designed schemes will be discussed in a somewhat deeper way.

It is worth remembering that the magnetic systems suitable in a e^+e^- storage ring may be well grouped in

three main classes, according to the direction of the magnetic field with respect to the beam line (see fig. 4.2.1.):

- longitudinal scheme: $\vec{B}$ parallel to the e^+e^- line
- trasverse scheme : $\vec{B}$ perpendicular to the e^+e^- line
- toroidal scheme : $\vec{B}$ linked to the e^+e^- line.

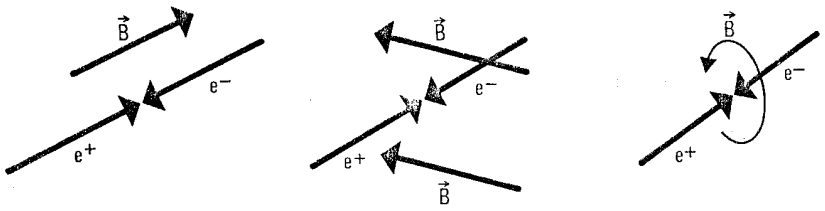

a) longitudinal b) trasverse c) toroidal

Fig. 4.2.1

The main features of these three types of magnets will be outlined in this sect. 4.2.1. The arrangements which seem more suitable for a SuperAdone ring will be discussed in more details in the following sections 4.2.2 and 4.2.3, keeping in mind some basic conditions which have been assumed as working hypotheses and which are summarized in table I.

TABLE I. Basic conditions for a SuperAdone general purpouse magnetic device.

- Straight section length	6 m
- Pipe diameter in the interaction region	10 cm
- Maximum electric power	5 MW
- Error in the sagitta measurement	0,2 mm

A| Longitudinal field magnetic systems

It is well known that the magnetic field induces a perturbation in the machine optics. Any magnetic shield around the vacuum pipe means a certain amount of material in the produced particles path which in general constitutes a trouble and anyway a deterioration of the quality of momentum analyzing detector. Therefore compensation mechanism is generally preferred according to a scheme sketched in fig. 4.2.2

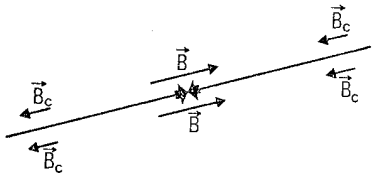

FIG. 4.2.2 - Compensation scheme for a longitudinal type of magnetic detector.

Another typical feature of the longitudinal (and the trasverse as well) scheme is that a magnetic flux return is needed, which means huge amounts of iron generally limiting the accesses to the useful volume and anyway reducing the flexibility of the device (for instance as far as the γ detection is concerned). The situation is sketched in fig. 4.2.3

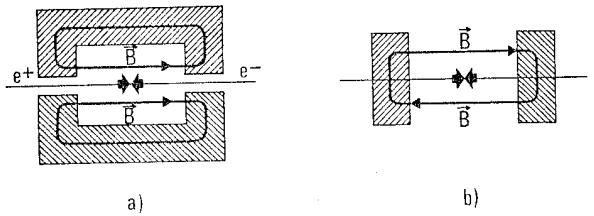

FIG. 4.2.3 - Iron magnetic field return systems in the case of longitudinal field configuration.

A longitudinal magnetic field configuration can be obtained in several ways, all making use of the basic solenoidal field structure. Three possible solutions are indicated in fig. 4.2.4 a), b) and c), where the principles of the pure solenoid, split solenoid and Helmoltz coils are respectively sketched.

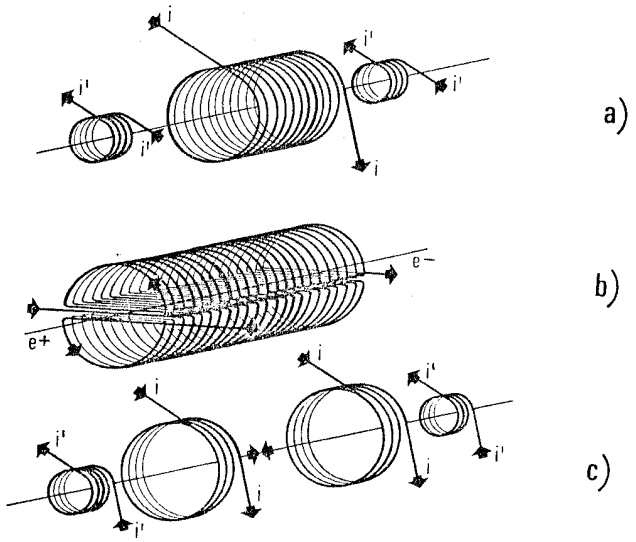

FIG. 4.2.4 - Schematic longitudinal field

In all of the above quoted arrangements, the longitudinal structure of the magnetic field results in bending the charged particles produced in the interaction region, according the transverse projection of the momentum with respect to the beam line (axis of the solenoid). This means that, due to the magnetic field, large variations of the azimuthal angle (φ) and small variations of the zenithal angle (θ) are expected within the useful volume of the detector.

$\vec{B}$| Transverse field magnetic systems.

Also in this case there is a perturbation to the machine which has to be accurately compensated according to the scheme of fig. 4.2.5. Any compensation system has the disadvantage

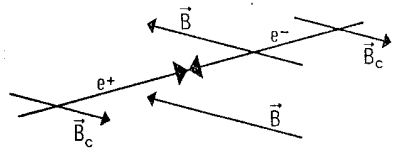

FIG. 4.2.5 - Compensation scheme in the case of a transverse magnetic field.

of inhibiting the access for detection of the small zenithal angle θ region. The problem of the magnetic flux return can be solved by the usual iron structures which can be pushed far apart from the beams; in this respect the situation is more convenient than in the case of the longitudinal devices. A

schematic view of a complete transverse field structure is shown in fig. 4.2.6

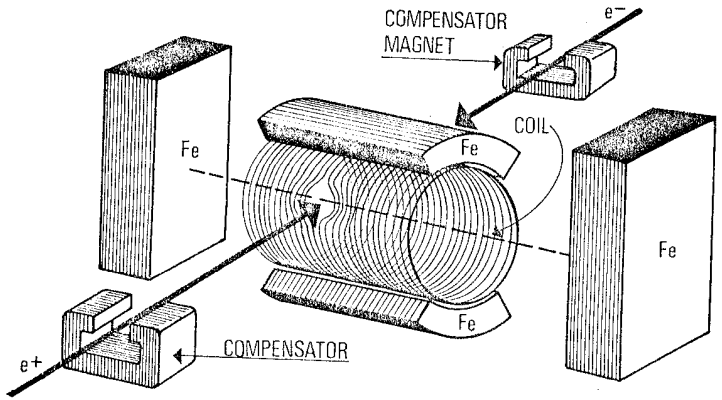

FIG. 4.2.6 - A schematic view of a transverse field system.

A serious problem, which is peculiar of the transverse magnets in a e^+e^- storage ring, deals with the low energy electromagnetic background following the beams. This background is bent by the magnetic field against the small θ angle region of the detector possibly causing critical operational conditions.

Beside the scheme shown in fig. 4.2.6, other arrangements in order to have transverse fields in the interaction regions may be carried out either as special bending elements of the machine structure [21] (and thus minimizing the compensation problems) or by coupling two opposite field uniform magnets as shown in fig. 4.2.7

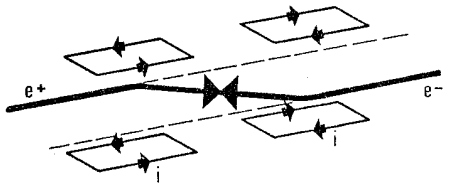

FIG. 4.2.7 - Split field magnet system. Compensation is needed in order to correct the beam displacement.

As a general comment to the transverse field systems it is enough to note that the charged particles are bent mainly because of their longitudinal momentum components, so that large θ variations are to be accurately measured in the momentum analysing volume; correspondingly small φ variations are produced by the magnetic field.

When realized with a solenoid (Adone-MEA solution) [1] the total solid angle available for momentum analysis cannot be very large (not larger than $\sim$ 50% x 4π). On the other side, a split field magnet large solid angle solution (ISR type of magnet) [2] does not allow a confortable γ rays detection, due to the limited volume available inside the gap of the magnet. A split field magnet may be well suited in the case of two - photon interaction processes, where the motion of the center of mass tends to concentrate the final state products within small θ angular regions around the beam line (thus producing kinematical situations not dissimilar from the ones typical in the ISR pp reactions).

c) Toroidal magnetic field system.

A toroidal magnetic field (see fig. 4.2.1,c) is generated by currents loops arranged on planes having the beam line as a common intersection as shown in fig. 4.2.8.

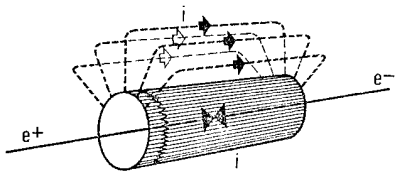

FIG. 4.2.8 - Toroidal magnetic field current generating system

A good cylindrical symmetry of the system around the beam axis is critically recommended in order to avoid any compensation. Along the beam line the magnetic field is zero and its radial dependence is shown in fig. 4.2.9.

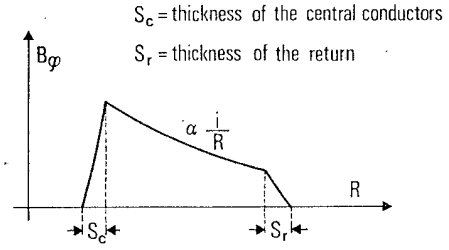

FIG. 4.2.9 - Toroidal field radial distribution.

If the current structure sketchedin fig. 4.2.8 is realized by a small number of coils, the magnetic field lines around the beams, as seen in a plane perpendicular to the beam axis, are shown in fig. 4.2.10 together with the resulting magnetic field radial distribution.

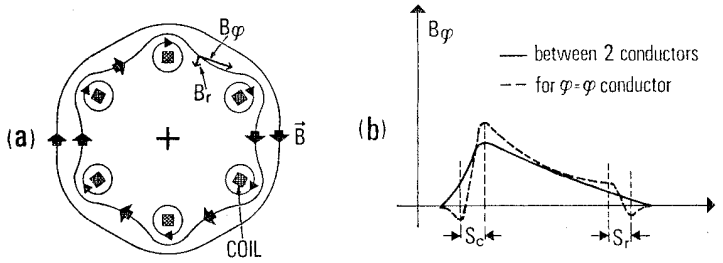

FIG. 4.2.10. - Toroidal magnetic field generated by a limited number of coils.

The field distorsion in the vicinity of the beam line is related to the requirement of cylindrical symmetry.

It is worth noticing that, in the case of toroidal field, no flux return iron is requested, this resulting in obvious advantages as far as the weight of the system, the access to regions free from material and the general flexibility of the system are concerned.

Another favourable situation deals with optimum use of the bending power of the magnetic field, due to the perpendicularity of the field lines with respect to the trajectories of the particles when produced in the interaction region.

This particular structure of the magnetic field gives this system the very relevant property of not influencing the φ emission angle of the produced particles (see fig. 4.2.11) thus supplying an immediate tool in order to achieve a fast rejection of background events (cosmic rays).

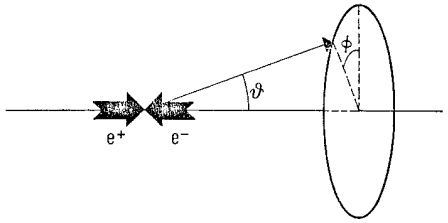

(a)

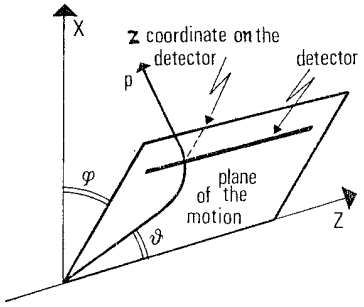

(b)

FIG. 4.2.11 - Geometry of the charged particle detection in a toroidal field device.

Some schemes of practical realizations are shown in fig. 4.2.12, where the rectangular boxes indicate the coils.

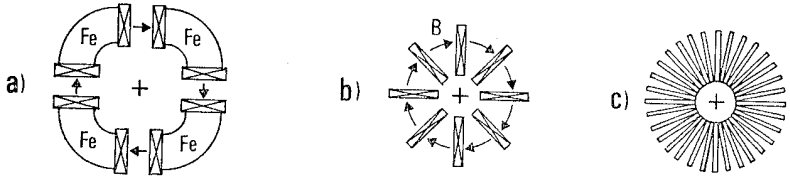

FIG. 4.2.12. - Schematic dispositions in order to have toroidal magnetic fields.

It is clear that a disadvantage of the toroidal scheme is represented by the parallel coil conductors running around the beam line which in most cases have to be penetrated by the particles before they enter the useful magnetic region.

In this respect any effort has to be made in order to reduce the thickness of the conductors near the beams to the minimum values consistent with the required high currents.

When comparing different magnetic devices a certain number of basic elements has to be kept in mind. The most important of such elements are summaried in table II.

TABLE II - COMPARISON OF THE DIFFERENT MAGNETIC DEVICES (a)(b)

MAGNETIC DEVICE				Interaction with the machine		Can charged hadrons get out of the magnet?							Total weight (in tons)	
name		machine situation (end 1973)	ref.	Does magnetic field perturbate the beams?	Is the coil linked with the machine?	in the $\Delta\Omega$ solid angle where p is measured	in the $\Delta\Omega$ solid angle compensated to 4 p	fraction of the total solid angle where the momentum can be measured	momentum resolution for $\theta = 90°$ p=1GeV/c	Bending power $\theta = 90°$ (in Tm)	total external dimensions (length x width x height) (in meters)	Maximum a'worked power (conventional coils)*	coils	the flux
Longitudinal solenoid	SPEAR	in operation	(3)	YES	(b)	(b)	(b)	.70	.020	.6	4x3x3	2.4	7.5	130
PLUTO	DORIS	in operation	3)(4)	YES	YES	NO	NO	.70	.025	1.2	2x4x3	supercond.		120
ZEUS	DORIS	project	(5)	YES	YES	YES	NO	.94	.015	1.6	5x6x7	2.6	57	700
Split solenoid	S.A.	evaluation	§4.2.2	NO	NO	NO	NO	.85	.008(c)	.8	6x3x3	5	31	32
Longitudinal solenoid	S.A.	evaluation	§4.2.2	YES	YES	NO	NO	.92	.010(c)	1.0	5x3x3	5	32	121
M.E.A.	ADONE	in operation	1) (3)	YES	NO	NO	NO	.44	.02 (c)	.3	3x4x3	2	3	80
Split-Field magnet	ISR	in operation	2) (3)	YES	NO	~ YES	~ NO	~ .8	.001 (c)(g)	12	10x3x7	6	42	840
DORIS	DORIS	project	(6)	NO	NO	YES	NO	.24	.022 (e)	1.0	4x3x3			90 (f)
ORTOPUS	DORIS	in constr.	(7)	NO	NO	YES	NO	.60	.009 (e)	2.4	4x5x5	supercond.	30	-
Composed toroidal	S.A.	evaluation	§4.2.3	NO	NO	YES	YES	.96	.02 (c)	.38	5x2x2	5	4	-
Supercond. toroidal	S.A.	evaluation	§4.2.3	NO	NO	YES	YES	.96	.08 (e)	.34	2x2x2	supercond.	.3	-

(a) When information is not available the corresponding cell of the table is left empty.
(b) Dashed cells indicate unwanted properties.
(c) Evaluation with a ± 0.2 m. error in the sagitta measurement.
(d) Evaluation at $\theta = 0°$
(e) Evaluation with a 7 mrad error on the deflection measurement
(f) Including the coils.
(g) $\Delta\Omega_p$ is the solid angle available for momentum analysis, whereas $\Delta\Omega_{ch,\gamma}$ indicate the avalaible solid angle where the detection of the charged particles and photons respectively is possible.

4.2.2. - Longitudinal magnets

Most of the magnetic systems so far realized or planned for Storage Rings are of the longitudinal class. We will discuss first some existing magnets (the SPEAR magnet as an example of longitudinal solenoid, and the concentrated coil magnet ZEUS, proposed for DORIS in DESY), then two possible schemes devised for SuperAdone, the "Split-Solenoid" as an example of longitudinal solenoid not linked with the machine, and a longitudinal solenoid of the SPEAR solenoid type having a wide angular acceptance.

I - SPEAR - Magnet[3]

We discuss very briefly this magnet, as its features are very similar to those of the longitudinal solenoid that we shall discuss later on. It is a longitudinal solenoid linked with the machine and compensated in the interaction region. A scheme of the structure of the solenoid and its detectors is shown in fig. 4.2.13. The essential parameters of the solenoid are reported in table II. The momentum measurement (with $\frac{\Delta p}{p} \sim 2\%$ at $\theta = 90°$ and $p = 1$ GeV/c) is achieved on a solid angle $\sim .7 \times 4\pi$ by 10 cylindrical magnetostrictive spark chambers with a maximum radius of 1.5 m. γ -rays can be detected outside the coil with a lead-scintillator sandwich system.

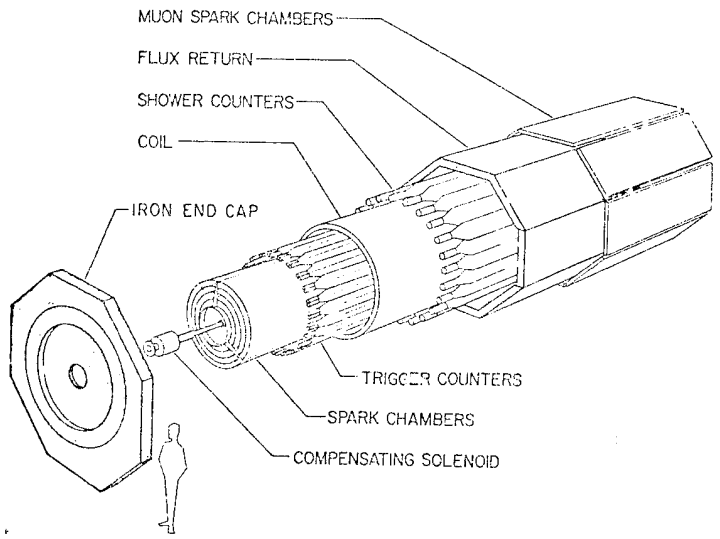

Schematic drawing of the SPEAR detector.

Fig. 4.2.13

The iron which closes the magnetic circuit is used as hadron filter, and a separation between hadrons, electrons, muons and photons can be obtained by a remote flat spark chamber system.

II - ZEUS[5]

ZEUS is the name of a magnetic system proposed for DORIS, consisting of two concentrated coils which produce a longitudinal magnetic field, reinforced by two

conical polar expansions (see fig. 4.2.14). Two smaller coils at the center of the polar expansions compensate the effects of the magnetic field on the beams. The return of the flux is obtained by means of two large iron plates, which serve also as mechanical support to the whole magnet (see again fig. 4.2.14), and leave entirely free two wide windows, 6x4.2 m^2 each, on both sides of the beam.

The conical expansions allow increasing the field around the interaction point by mantaining a large $\Delta\Omega p$ Far from the beams the field decreases but it retains its cylindrical symmetry around the beam axis (see fig.4.2.15). Therefore, to keep a high momentum resolution the magnet size must be very large: in particular the useful magnetic volume is $\sim$ 180 m^3. Also the proposed detector must be very large: the external cylindrical chamber has a $\sim$ 4 m. diameter and requires $\sim$ 7000 proportional wires to get a $\frac{\Delta p}{p}$ = 1.5% at $\theta = 90°$ and p = 1 GeV/c (which drops to $\sim$ 20% at $\theta \leq 37°$).

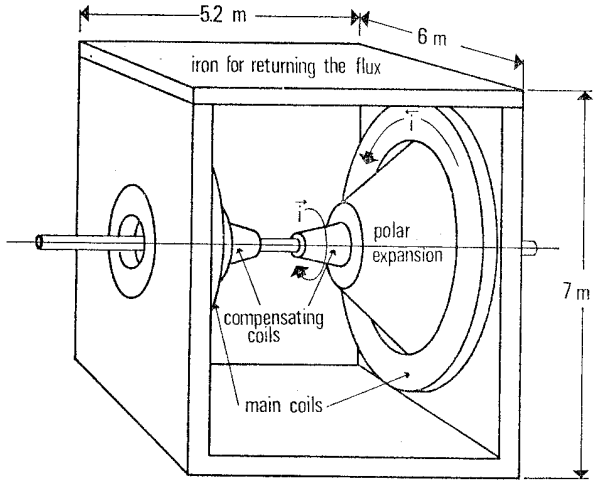

Fig. 4.2.14
The ZEUS magnet

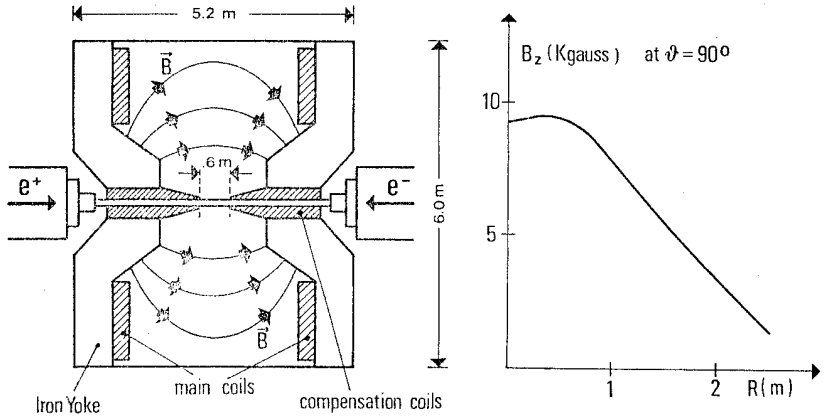

Fig. 4.2.15

Following the general requirements in section 4.1 the following remarks are in order concerning ZEUS:

1 - It has a good solid angle acceptance ($\Delta\Omega_p \simeq \Delta\Omega_{ch} = .94 \times 4\pi$)

2 - There is no material on the trajectories

3 - It is completely open on a wide solid angle ($\Delta\Omega_{Open} \simeq \frac{1}{2}\Delta\Omega_{ch}$)

Nevertheless:

4 - It is difficult to provide γ detection on a wide $\Delta\Omega_\gamma$, both because of the difficult arrangement of the γ detector around the conical poles, and because of the huge dimensions of the γ detector ($70 \sim 80$ m^2). The size of the γ detector can be reduced only at the expense of the space available to momentum measurement with a good resolution.

5 - Also the solid angle which the reaction products can go through freely can hardly be covered by devices for particle analysis (Cerenkov counters, range telescopes, ...), unless reducing the available space for momentum measurement.

6 - All particles emitted with $\theta < 20°$ are in any case lost in the compensating coils.

III - Split-Solenoid

This magnet is obtained by applying the split-field magnet principle to a solenoid. The main advantage of this scheme is that the magnetic field is closed on itself through the two iron end caps at the ends of the solenoid.

The main disadvantage is that the particles enter the magnetic field traversing the coil; the measurements on charged particles must indeed be separated in two parts: the measurement of the angles θ and φ before the conductor, and the momentum measurement in the magnetic field.

A solution for SuperAdone with Aluminium conventional coils (see fig. 4.2.16) has the characteristics shown in table III

Table III

Characteristics of the Split-Solenoid with conventional Aluminium coils.-

Length of the coil	= 400 cm.	
External radius of the coil	= 140 cm.	
Length of the magnet	= 560 cm	
Weight of the aluminium	= 31.4 t	
Weight of the iron	= 32 t	
$\Delta\ \Omega_{ch}$ (geometric)	= .86 x 4 π	
$\Delta\ \Omega\ \gamma$ (geometric)	= .77 x 4 π	
Resistance	= .56 $\mu\Omega$	(with a
Total current	= 3 MA	5 MW Power supply)
Magnetic field	= 9,4 Kgauss	
$\frac{\Delta p}{p} \simeq .8\% \times p \times \text{sen}\ \theta$ (with σ (sagitta) = $\pm$.2 mm)		

Though in the split-solenoid scheme there is no iron around the coils the thickness of the coils itself (30 cm of Al) is such that the γ's cannot be easily detected outside; indeed they must be either detected inside the coils, or the coils must have layer structure with γ-detectors in between. This problem can be solved by reducing the field by some factor so reducing the thickness of the coils. The momentum resolution is then worse by the same factor.

Besides γ detection, a difficult problem is how to fill the huge volume inside the coils (15 m^3) with very precise detectors.

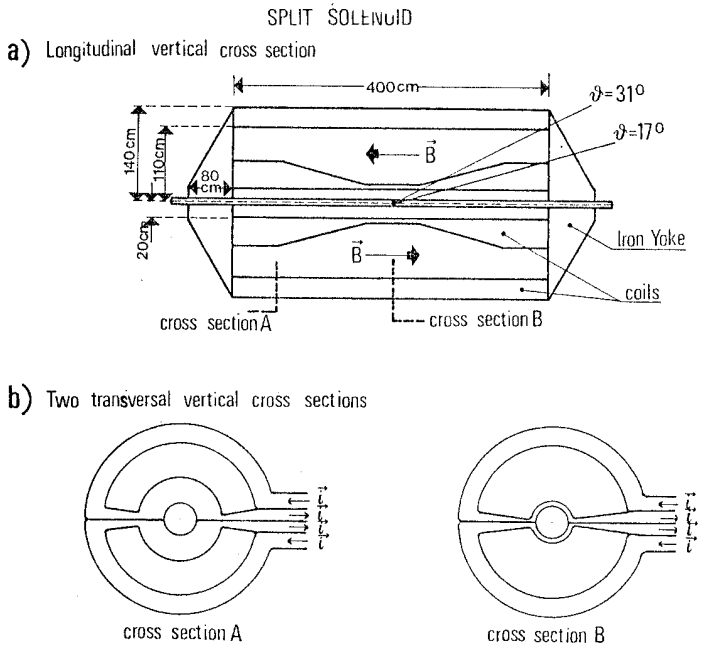

Fig. 4.2.16 - Split solenoid
(a) longitudinal vertical cross section
(b) two transversal vertical cross sections

Both problems (huge dimensions of detectors and thickness of the coils) should be easier to solve by using superconducting coils to get the maximum field ($\sim$ 20 Kgauss) allowed by the iron saturation. In any case this solution can be used only if the thickness of the whole coil (superconductor, thermal shieldings, vacuum tank) around the interaction region can be limited to 2 ÷ 3 cm of equivalent aluminium. This possibility is still open and we have not yet done any detailed study on it.

IV - Longitudinal solenoid.

A preliminary study to define the gross features of a longitudinal solenoid has been performed. Also, solutions concerning the detection system have been considered. We deliberately discarded the possibility of constructing a superconductor device which is left to further analysis of the problem.

The main body of a longitudinal magnet consists of an aluminium cylindrical coil with its axis coinciding with the beam line in the ring. An iron return yoke completes the magnetic circuit, as shown in fig. 4.2.17: it consists of a cylindrical mantle with two stoppers at the ends. Some elements of the detection system (γ detectors) can be arranged into the space between the coil and the iron.

In Table IV the main parameters of some of the solutions considered are shown. The last solution indicated in this table looks adeguate to the requirements summarized in section 4.1. Therefore we centered our attention on it in this study. This is a reasonable compromise between the need of a large solid angle (0.92x4π with magnetic analysis) and of a good momentum resolution (5% at 5 GeV).

What follows is based on the simplifying assumption that only pions are produced. The events have been generated by a Montecarlo in which the maximum particle number is 10 and the momenta are phase-space distributed.

Table IV

$\Delta p_\perp / p_\perp$ a 5 GeV/c	$\Delta\Omega/4\pi$	B (KGauss)	li (m)	ri (m)	s (cm)	Weight		# (GeV)
						Coil (tonn)	Iron (tonn)	
0.5%	.66	14	4.0	2.15	40	69	969	2.8
0.5%	.60	10	3.8	2.41	36	56	754	4.0
0.5%	.60	12	3.4	2.30	41	52	766	4.0
1%	.74	10	4.0	1.73	41	48	382	3.2
1%	.77	12	4.0	1.59	36	39	398	4.1
2%	.83	10	4.0	1.35	41	35	189	3.4
2%	.83	10	4.0	1.35	31	17	189	4.4
2%	.85	12	4.0	1.15	31	24	199	4.1
5%	.92	14	4.0	0.85	40	32	121	3.4

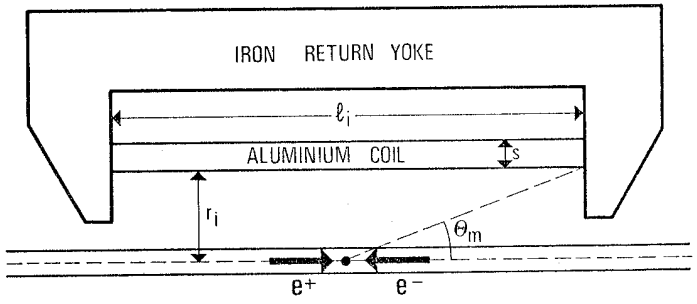

Fig. 4.2.17

We assumed that:

i - The error in the sagitta is 0.2 mm

ii - The error in the depth is 4 cm

iii - Charged pions of any energy are detected

iv - The minimum angle for charged pion detection (θ_m) is 10° (from the beam axis) although with smaller accuracy because of the sagitta being shorter than in the case of full magnetic analysis.

v - Detection of secondary γ's from Π° decay in the solid angle subtended by the coil. The efficiency is assumed to be 90% with a minimum γ energy of 100 MeV.

vi - The useful radius for momentum measurement is the coil radius r_i minus 20 cm deserved for γ detection.

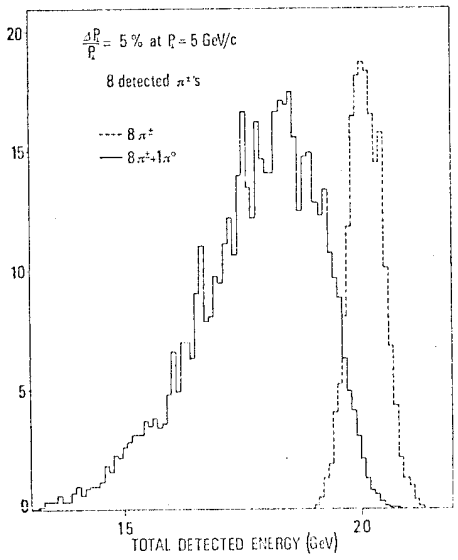

Fig. 4.2.18

Figure 4.2.18 shows the total energy distribution for the case in which 8 charged pions are detected in events with 8 or 9 produced particles. The geometrical efficiency for this case is about 80%. The distributions shown in fig. 4.2.18 are clearly not normalized.

By comparing these distributions, it is seen that the contamination of the 8 charged pion channel due to the channel in which 8 charged + 1 neutral is produced can be made reasonably low. Therefore, with maximum charged multiplicity the discrimination is possible even with no γ detection. This possibility obviously improves at lower multiplicities. However, the contamination is much higher for 2 π° produced in addition to 8 charged π's assuming no γ detection.

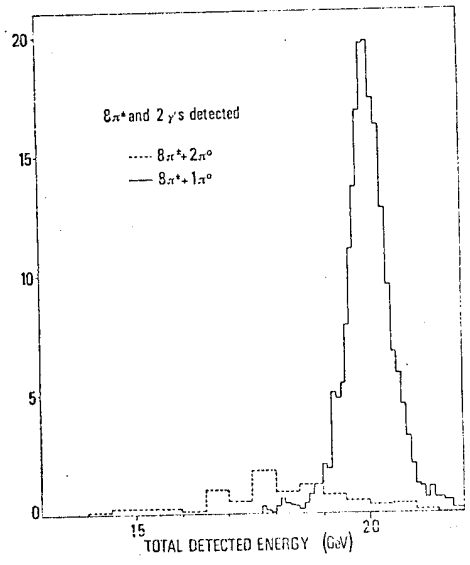

Fig. 4.2.19

Figure 4.2.19 shows the total energy distribution after detection of a pair of γ's from the same π° in the production of 8 $\pi^{\pm}$ + 1 π° and 8 $\pi^{\pm}$ + 2 π°. Spectra are normalized to detection efficiencies for comparison.

We note here, on the basis of the require - ments mentioned in section 4.1, that:

a - The charged particles cannot traverse the coil so that the π - K distinction by gas Cerenkov counters is not possible.

b - The measurement of γ energy is not conceivable unless much space inside the coil is utilized for this giving correspondingly up the useful space for momentum measurement.

c - Two-photon reaction detection is unfavoured by the longitudinal field and the presence of the end stoppers.

Concerning the apparatus, we see that the large solid angle extending down to θ = 10° from the beam axis makes the use of spark chambers unpractical. Up to day, possible techniques to be considered are:

α - Multiwire proportional chambers

β - Drift chambers

γ - Streamer chambers

because of their isotropy. Discarding the last case (streamer ch.) in view of the optical problems with this magnet structure, we consider the two alternatives α and β .

α - Proportional chambers. Assuming 2 mm separated wires (that is 0.7 mm error at the point) one needs 25 wire layers to get .3 mm error on the sagitta. All together, the number of wires is 40.000 and the resolution in momentum 7.5% at 5 GeV.

β - Drift chambers. With 5 cm spaced wires and assuming a 0.35 mm point error, in order to get an error of 0.2 mm on the sagitta we need 8 wire layers. In this case the total wire number is down to 4000 and the momentum resolution is 5% at 5 GeV. It is any way to be noticed that the use of drift chambers in a high magnetic field is still an open problem.

For the detection of neutrals, a possible suggestion is to add some wire layers inside and outside the coils together with shower plates. This problem will be reconsidered in subsection 4.2.5.

4.2.3 - Toroidal magnets

A toroidal field system, consisting of 6 radial sliced yoke magnets has been proposed (with the name ORANGE) for DORIS at DESY[6]. It will not be discussed here as it does not correspond to the criteria stated in sec. 4.1 (for its $\Delta \Omega p \sim 0.24 \times 4\pi$).

We discuss instead the toroidal magnet OCTOPUS (also proposed for DORIS), consisting of some superconducting coils disposed in radial planes through the beam axis; and two versions of toroidal magnets with "nearly continuous" coils, conceived on purpose for Super Adone, the first (the composed toroidal magnet) with three Aluminium coils, the second (the superconducting toroidal magnet) with a single superconducting coil.

I - OCTOPUS [7]

The toroidal magnetc field is produced by a total current "i" distributed among a small numbers (8) of superconducting coils.

The scheme of the magnet is reported in fig.4.2.20 (a) (b). The "φ component" of the toroidal field as a function of R is not uniform in φ (see fig. 4.2.21), but its bending power, $\int B.dl$, does not vary with φ. Therefore the field works on the θ angular coordinate, and the main feature of the toroidal field is preserved; in fig.4.2.22 it is shown how easy is a fast momentum selection.

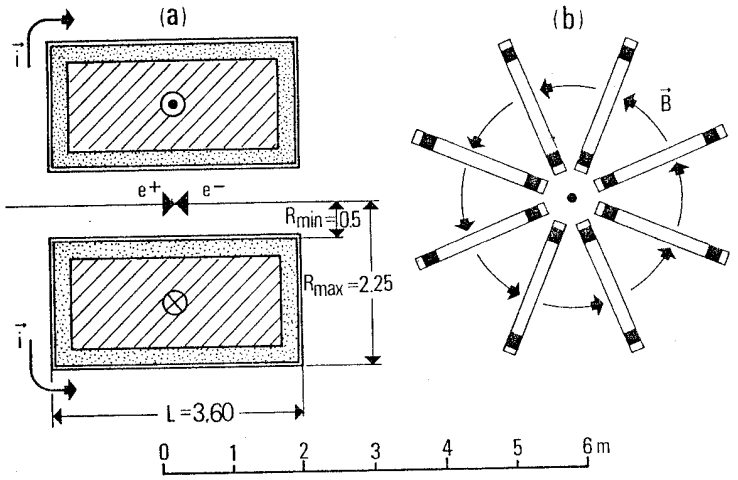

Fig. 4.2.20

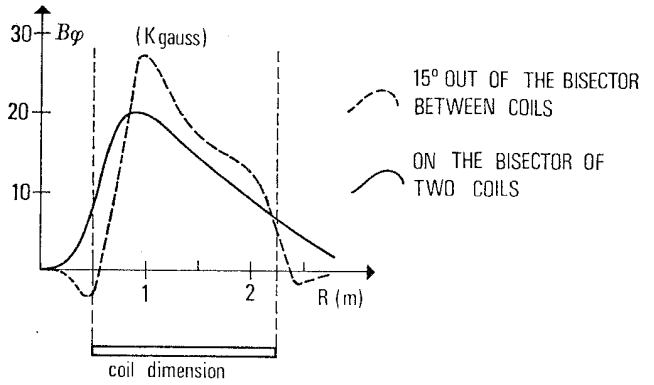

Fig. 4.2.21

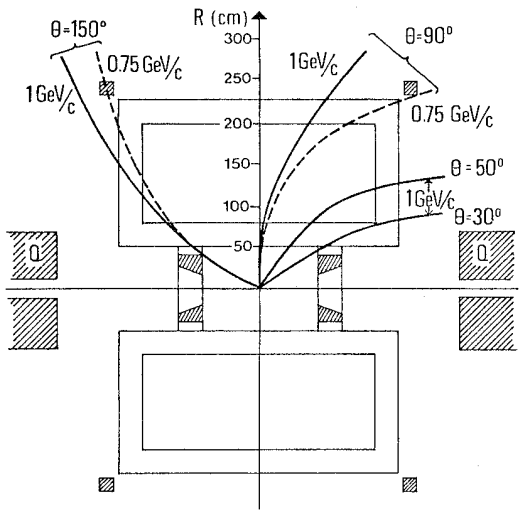

Fig. 4.2.22

According to the requirements in sec. 4.1, we make the following remarks about OCTOPUS:

1 - The thickness of the coils prevents from obtaining a $\Delta\Omega p$ near to $\Delta\ \Omega_{ch}$: in fact to diminish the minimum radius R_{min} from the beam axis occupied by the coils (see fig. 4.2.22) while corresponds to a better $\Delta\ \theta$ necessarily reduces $\Delta\ \varphi$; the contrary happens when R_{min} is increased. This limits the solid angle for the momentum measurement to $\Delta\ \Omega\ p \sim 0.6 \times 4\ \Pi$.

2 - A good momentum resolution is alternative to a wide

$\Delta\Omega\gamma$: in fact, when the whole magnetic volume is used for momentum measurements the surface covered by the γ detector for a large $\Delta\Omega\gamma$ becomes very large ($\sim 80\ m^2$) and in any case $\Delta\Omega\gamma \leq \Delta\Omega p \leq 0.6 \times 4\ \pi$.

3 - Again for geometrical reasons a good momentum resolution is alternative to any analysis on the nature of the particles.

II - TOROIDAL MAGNET WITH "NEARLY COUNTINUOS" COILS

A nearly continuos coil in the azimouth φ allows to dismi nish R_{min} and indeed the length and the diameter of the coil itself covering the same $\Delta\theta$.

However some material is introduced along the trajectories; then we must look for an useful compromise between the thickness of this material and the maximum magnetic field which can be obtained for a given maximum current density and power supply.

For a conventional aluminium coil it is convenient to choose a thickness $s \simeq 2$ cm; this corresponds to a $\sim$5% interaction probability, which leaves more than 1/2 of the 6 charged prongs events (to give an example) without any interaction. Allowing a current density $\phi \simeq 40\ A/mm^2$ we get B = 10 Kgauss for R=20 cm (see fig. 4.2.23).

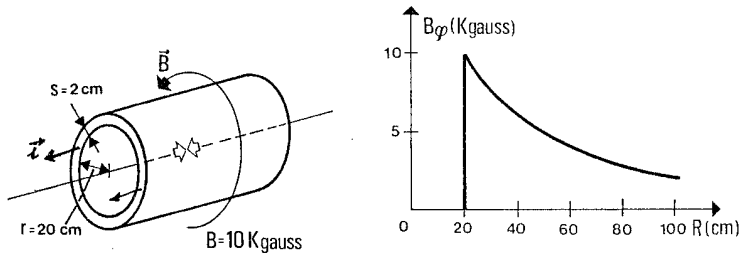

Fig. 4.2.23

For $\theta \lesssim 30°$ the thickness encountered by the particles becomes too high, and the part of conductor with a high current density becomes too long; the conductor must indeed be deformed (fig.4.2.24) or the coil must be subdivided in three separated coils, one covering $\Delta\theta \simeq 30° \div 150°$ and the other two down to the smallest angles (see fig. 4.2.25). To make this subdivision we used the property (see § 4.2.1 C) that the field is confined in the coil producing it.

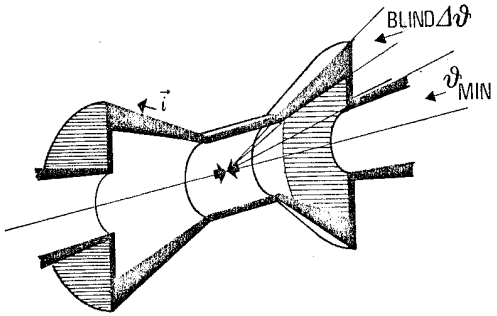

Fig.4.2.24
Deformed Central conductor (longitudinal cross section).

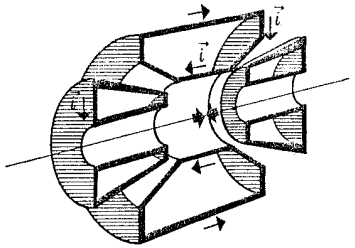

Fig.4.2.25
Three separated coils (longitudinal cross section).

To give practical estimates we choose this second solution, called in the following "composed toroidal magnet", since in this case the huge detection system is divided in three simpler devices. Also, we note that the acceptance at small θ's can be possibly changed by translation of the two small θ magnets along the beam direction.

II a - COMPOSED TOROIDAL MAGNET

The longitudinal vertical cross section of the magnetic system with its detectors for charged particles and γ's is given in fig. 4.2.26 (a); in fig. 4.2.26 (b), we separately show the magnets and their geometrical size.
The essential parameters of the system are given in table V separately for the central magnet M 1 and the magnets M 2 and M 3 (see fig. 4.2.26 b)). With the parameters shown in table V we get the momentum resolutions reported in fig. 4.2.27.

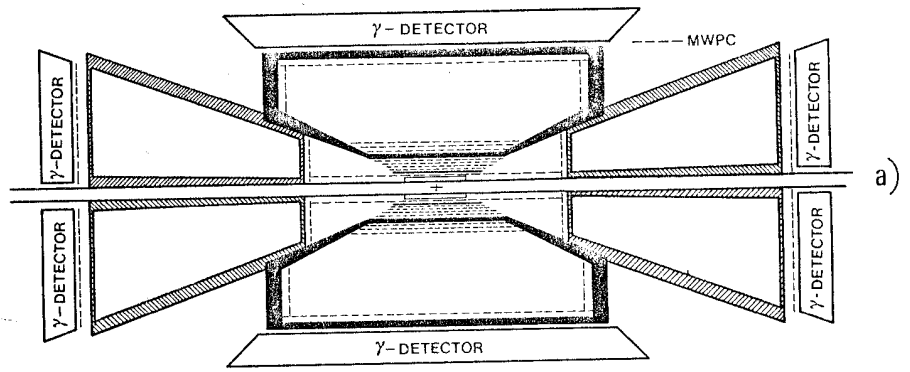

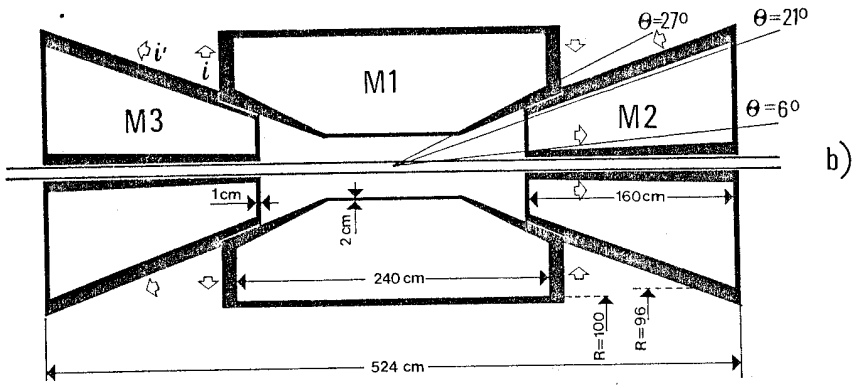

Fig. 4.2.26(b)

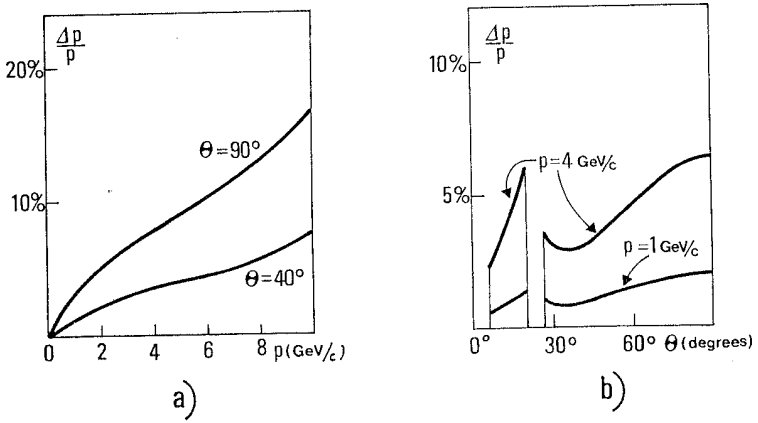

T A B L E V - Parameters of the composed toroidal magnet

		M1	M2(and M3)	M_1	M_2(and M_3)
Coils:	length (external)	260 cm	164 cm	3 t	1 t
	Rmax (external)	105 cm	110 cm	3 MW	1 MW
	Δ φ (geometrical)	360°	360°	Total current 1.27 MA	0.47 MA
	Δ θ (geometrical)	27° ÷ 154°	6° ÷ 21°	B(maximum) 11.5 Kgauss	9.7 Kgauss
	$\Delta\Omega_p/4\pi$ (geom.)	.85	.03	Al thickness in the trajectories: input: 2 cm, output: 5 cm	≤ 2 cm, ≤ 2 cm

Detector for charged particles:

	M_1	M_2(and M_3)
- development of the longitudinal coord. to be measured:		
2 planes in 2 sector with a ± 0.2 mm precision total development	60 cm	60 cm
2 planes in 2 sector with a ± 0.3 mm precision "	640 cm	130 cm
2 planes in 2 sector with a ± 0.5 mm precision "	1060 cm	360 cm
4 planes in 2 sector with a ± 0.5 mm precision	3600	1600
- Number of proportional wires for φ measurement	~ 1000	~ 500
- Number of proportional wires for ambiguity resolution		
γ detector : surface to be covered	23 m^2	3 m^2

According to the requirements quoted in section 4.1, we must add the following remarks:

1 - The magnetic system well satisfies the requirements on $\Delta\,\Omega_{ch}$, $\Delta\,\Omega\,\gamma$, $\Delta\,\Omega\,p$, whereas to obtain a $\frac{\Delta\,P}{p} \lesssim 10\%$ up to ~ 5 GeV/c the measurement accuracies must be very good (a $\pm$ 0.2 mm on the "sagitta" is required).

2 - 80% of the detected particles can be analyzed after the magnets, but directions must be redefined to take the scattering into account.

3 - After the magnets the energies of the γ's can be measured with a reasonable accuracy also for the γ's that converted in the coils.

4 - The angular range which is not useful for momentum measurement, is 21° ÷ 27°, far away from the beam axis: this allows the study of the two-photon reactions with products at $\theta \geq 6°$ (or also $\theta \gtrsim 3.5°$ without changing any important parameter); by translation of the M2 and M3 magnets along the beam direction the minimum accepted angle can go down to 2°.

II b - SUPERCONDUCTING TOROIDAL MAGNET

For a superconducting toroidal coil the following choices are advisable:

1) a single coil, as simple as possible
2) no detectors inside the coil in order to contain the coil itself in a single dewar.

It follows that to coverning small θ angles the coil must be very long and all the thicknesses must be minimized. For an evaluation of possible parameters we assume:

a) dimensions of the coil: length = 200 cm, inner radius = = 20 cm and outer radius = 80 cm.
b) coil contained in a single dewar, as in fig. 4.2.29.

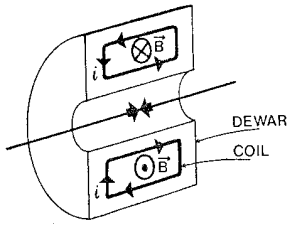

FIG. 4.2.29

c) superconducting wire bound to an aluminium matrix, with the following characteristics:
   - total thickness of the coil on the inner cylinder equivalent to 1.2 cm of aluminium
   - maximum current density = 100 A/mm^2 at 1.3 Tesla (in the OCTOPUS magnet it was 90 A/mm^2 at 4 Tesla [7])
   - maximum field = 1.27 Tesla (in the OCTOPUS magnet it was 4 Tesla)

d) thickness of the insulation 2 cm (as in the OCTOPUS magnet) on the inner cylinder and 3 cm on the outer cylinder

e) total thickness on particle trajectory at $\theta = 90°$ equivalent to 24 mm of aluminium (18 mm on the inner cylinder and 6mm in the outer one); the corresponding interaction probability for pions amounts to $\sim$ 6%.

The realization of such a light structure which must be able to support the pressure of the field on the inner cylinder ($\leq$ 5 atm) and the atmospheric pressure is a difficult technical problem. A possible structure is formed of two half-cylinders, each consisting of a single piece of aluminium lodging the superconducting cable and supporting the vacuum tank and the detectors, as sketched in fig. 4.2.30; some plates and connecting rods distribute to the outer cylinder the most part of the pressure applied to the inner cylinder.

The vertical cross section of the magnetic system with the detectors is shown in fig. 4.2.31 (a); in fig. 4.2.31 (b), we show in some detail the magnet and its mechanical structure.

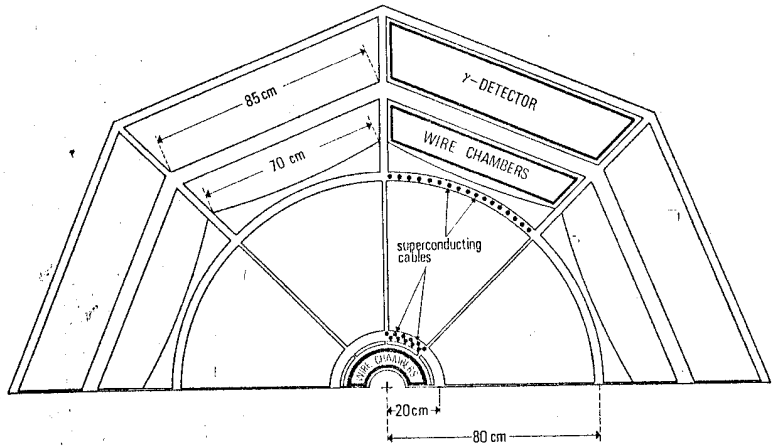

Fig. 4.2.30

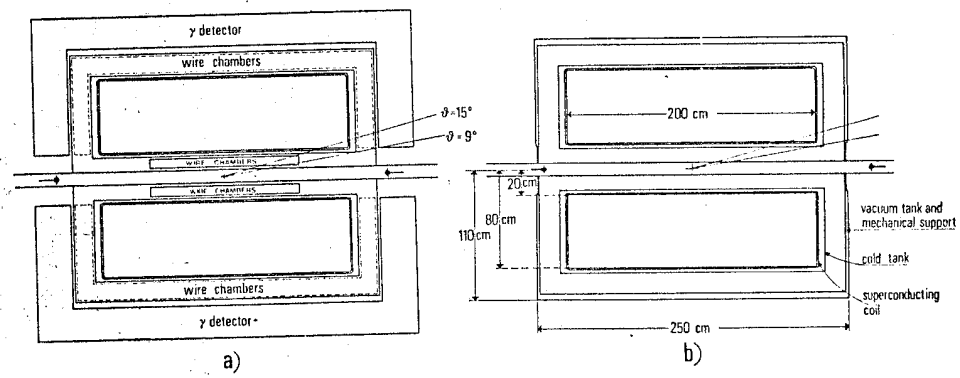

Fig. 4.2.31

According to the requirements quoted in section 4.1, we must add the following remarks:

1 - The magnetic system well satisfies the requirements on $\Delta\Omega_{ch}$, $\Delta\Omega\gamma$, $\Delta\Omega p$, whereas to obtain a $\frac{\Delta P}{P} \lesssim 10\%$ up to ~ 5 GeV/c the measurement accuracies must be very good (a $\pm$ 0.2 mm on the "sagitta" is required).

2 - 80% of the detected particles can be analyzed after the magnets, but directions must be redefined to take the scattering into account.

3 - After the magnets the energies of the γ's can be measured with a reasonable accuracy also for the γ's that converted in the coils.

4 - The angular range which is not useful for momentum measurement, is 21° ÷ 27°, far away from the beam axis: this allows the study of the two-photon reactions with products at $\theta \geq 6°$ (or also $\theta \gtrsim 3.5°$ without changing any important parameter); by translation of the M2 and M3 magnets along the beam direction the minimum accepted angle can go down to 2°.

II b - SUPERCONDUCTING TOROIDAL MAGNET

For a superconducting toroidal coil the following choices are advisable:

1) a single coil, as simple as possible
2) no detectors inside the coil in order to contain the coil itself in a single dewar.

It follows that to coverning small0 angles the coil must be very long and all the thicknesses must be minimized. For an evaluation of possible parameters we assume:

a) dimensions of the coil: length = 200 cm, inner radius= = 20 cm and outer radius = 80 cm.
b) coil contained in a single dewar, as in fig. 4.2.29.

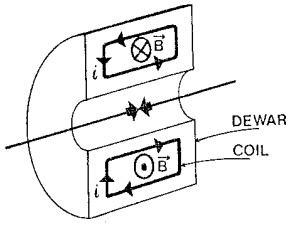

FIG. 4.2.29

The main parameters are reported on Table VI. The mechanical problems concerning the support of the coil weight are simpler as compared to the pressure problem; also the access to the apparatus can be made easy by the separation in two (or possibily more than two) sectors including the detectors.

The complexity and the dimensions of the detectors are quite reasonable, but for the small device for measurement of angles around the interaction point which must be very compact and precise ($\sim \pm$ .3 mm at each point). With the parameters for charged particle detectors reported in table VI the momentum resolutions are those reported in fig. 4.2.32.

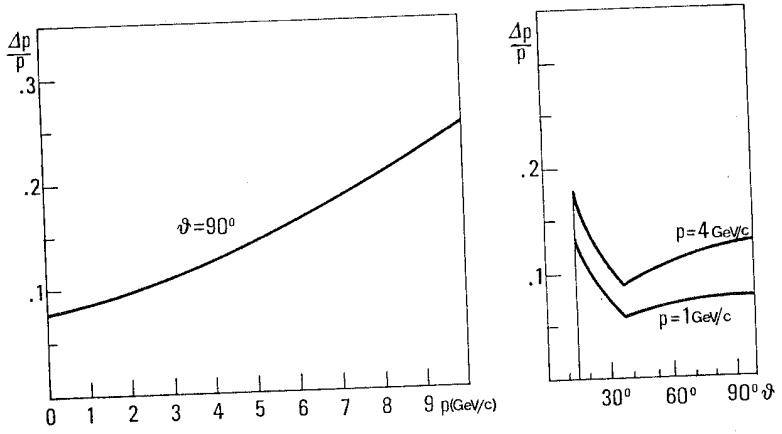

Fig. 4.2.32

TABLE VI - Parameters of the Superconducting Toroidal Magnet System.

Coil	length (external)	204 cm
	maximum radius (external)	82 cm
	$\Delta\Omega_P$ (geometrical)	.96 x 4 π
	$\Delta\Omega_\gamma$ (geometrical)	.98 x 4 π
	total current	1.27 MA
	maximum field	1.27 Tesla
	maximum magnetic pressure	5 atm
	volume of the superconducting cable	.0654 m^3
	weight of the superconducting cable	260 Kg
	total thickness at $\theta = 90°$ equivalent to	2.35 cm of Al
Charged particle detectors	longitudinal coordinate with a $\pm$ .3 mm precision (4 planes in 2 sectors) $\sim$ 14 m
	with a $\pm$ .5 mm precision (4 planes in 2 sectors) $\sim$ 27 m
	number of proportional wires for azimuth measurement $\approx$ 3200
	number of proportional wires for ambiguity resolution $\approx$ 1000
γ detectors: total surface to be covered	$\sim$ 17 m^2

Furthermore, according to the requirements quoted in section 4.1 the following remarks can be made:

- The apparatus well mets the requirement of large solid angles $\Delta\Omega_{ch}$, $\Delta\Omega\gamma$ and $\Delta\Omega_{p}$; in particular $\Delta\Omega_{\gamma}$ can be pushed to .98 x 4π. However it is difficult to get a $\frac{\Delta P}{P} < 10\%$, as the multiple scattering introduces a $\sim$ 8% contribution, nearly constant with the momentum which cannot be easily reduced.
- Concerning the particles which do not interact in the magnet ($\sim$ 90% of the total) π/K distinction can be obtained outside the magnet by using a Cerenkov counter system; in this case the γ detector must be either removed or displaced further away and therefore distributed on a larger volume.
- The "dead angle" for charged particles can be likely small enough (between $\theta \sim 15°$ and $\theta \sim 9°$) such that charged particles emitted at $\theta < 9°$ can be detected; this may allow the detection of final products of 2 γ-channel interaction.

4.2.4 - Particle identification

The nature assignement to the non hadronic charged particles (electrons and muons) may be performed by making use of their different behaviour when passing through matter. The usual hadronic filters, made by a series of heavy slabs with proper detectors in between, let the muons pass through without suffering interactions and the electrons exploit their showering attitude. As far as the electron induced electromagnetic showers are concerned, the problem is strictly connected to the photon detection and will be discussed in the sect. 4.2.5.

Therefore the question remains on how to discriminate among charged hadrons (π, k, p) whose momenta are supposed to be known within accuracies of the order of 5%. A basic piece of information, in order to discuss how to achieve such a discrimination, is the momentum distribution of the produced hadrons in a multihadron $e^+ e^-$ annihilation process. Under the assumption of an invariant phase space momentum distribution, a typical 8 π'S production reaction at 20 GeV total c.m. energy generates the momentum distribution shown in fig. 4.2.33.

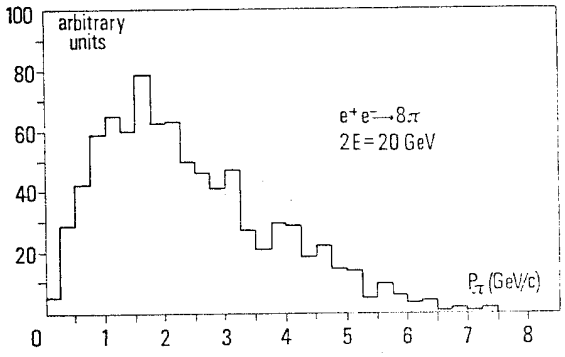

Fig.4.2.33
Pion momentum distribution according to an invariant phase space momentum distribution calculation for the reaction $e^+e^- \to 8\pi$ at a total c.m. energy of 20 GeV.

A relevant feature of this momentum distribution is that about half of the pions have momenta below 2 GeV/c. In this low-momenta range the correct assignement of the nature of the particle is particularly needed when the total energy carried by the particle has to be determined (the ambiguity on the mass value m_π or m_k in the relationship $\sqrt{p^2 + m^2}$ leads to uncertanties larger than the ones due to the measurement of the momentum).

The above requirement on π/k discrimination is obviously essential when exclusive channels are under investigation. In the case of inclusive reactions the $\pi/k/p$ discrimination has to be achieved up to the maximum available momentum even if in a limited fraction of the total solid angle ($(10 \div 20)\%\ 4\pi$).

The most suitable detectors, in order to discriminate among π , k and p, are proper combinations of velocity selectors based on the Cerenkov thresholds in different materials.

[It might be useful to recall the basic formulas governing the Cerenkov effect, namely

$$\frac{d N_\gamma}{d x} = 2 \pi \alpha \int \left(1 - \frac{1}{\beta^2 n^2}\right) \frac{1}{\lambda^2} d\lambda$$

which gives the number of photons emitted per unit length;

$$\cos \theta = \frac{1}{\beta n}$$

which gives the angular aperture of the Cerenkov light cone;
and that, in the case of gases, the pressure is proportional to $(n-1)$.

Table VII shows, for different materials, the values of the refraction index n, the number N_γ/cm of photons produced per cm by a $\beta=1$ particle, and the momentum thresholds for π's, k's and protons respectively.

By using a series of three different Cerenkov radiators a π/k discrimination turns out to be possible in the entire momentum region covered in spectrum of fig. 4.2. .33.

TABLE VII

MATERIAL	n	N_γ/cm	THRESHOLD (GeV/c)		
			π	K	P
PERSPEX	1.49	250	0.12	0.45	0.85
WATER	1.33	200	0.16	0.55	1.10
LIQUID AIR	1.210	140	0.20	0.72	1.40
LIQUID N_2	1.205	140	0.20	0.72	1.40
LIQUID H_2	1.097	75	0.31	1.10	2.10
LIQUID He	1.0206	19	0.70	2.50	4.60
C_5H_{12} GAS 1 ATM	1.0018	1.6	2.30	8.50	15.5
ISOBUTAN " "	1.0015	1.3	2.60	9.10	17.7
FREON " "	1.0013	1.2	2.80	9.70	18.4

The momentum region 0-0,5 GeV/c is well covered by a reasonably thin lucite Cerenkov counter. In the momentum range 0,5-2,0 GeV/c criogenic Cerenkov counters may solve the problem as it is shown in fig. 4.2.34.

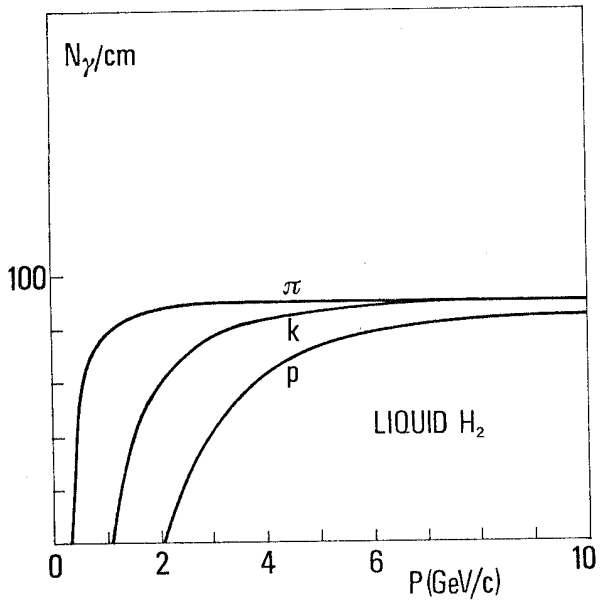

Fig. 4.2.34

The relatively high number of photons per cm makes possible small and compact arrangements suitable to be installed closely surrounding the vacuum chamber of the storage ring. For momenta above 2 GeV/c gaseous radiators are needed and the response of some suitable gases is sketched in Fig. 4.2.35.

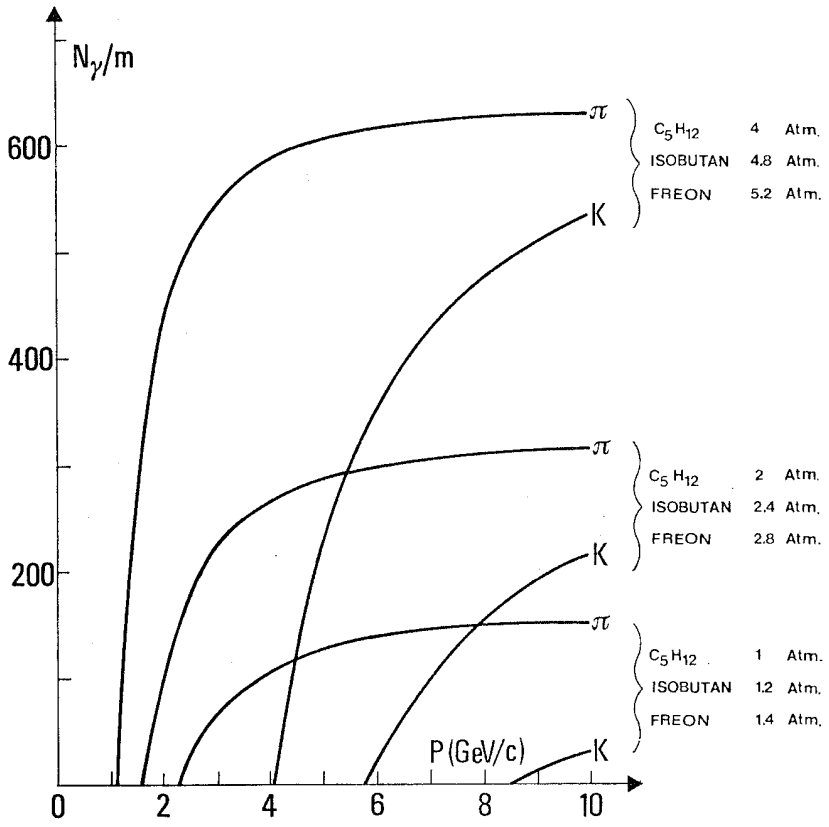

Fig. 4.2.35

Cerenkov light responses in photons/meter in the S_{11} photocathode wave length typical window for different gaseous radiators as a function of the incident momentum.

In view of a practical use of the quoted Cerenkov

materials in a Super Adone, many purpose, large solid angle, magnetic device, it seems easy to locate a large area lucite Cerenkov selector, properly hodoscopised, immediately surrounding the cylindrical magnetic volume. With typical covered areas of the order of 30 m^2 the whole useful solid angle may be covered.

As far as the criogenic Cerenkov device is concerned (0,5-2,0 GeV/c momentum range) it has been already mentioned that, due to the peculiar problems of the low temperature working objects, the most convenient solution seems to be a compact device very close to the interaction region in a such a way to be able to cover a large solid angle by a relatively small detector. Therefore this criogenic Cerenkov counter should be met by the particles before they start being deflected in the magnetic volume. From the point of view of the practical realization criogenic Cerenkov detectors were known to give satisfactory performances[8][9]. Further studies on a small size liquid H_2 counter have been recently performed in Frascati[11] with the aim of testing the light collection efficiency in an arrangement particularly suited for the Super Adone kind of situation. The encouraging results of this preliminary work are shown in fig. 4.2.36 (sketch of the set up as tested at the 1 GeV electrons of the Frascati electronsynchrotron) and fig. 4.2.37 (efficiency measurements for different high voltages supplied to the photomultiplier). The conclusions are that a cylindrical liquid H_2 Cerenkov counter surrounding the vacuum pipe of the experimental region of the storage ring seems conceivable as far as its performances are concerned. Furthermore the thickness of such detector can be reduced to acceptable values in order to minimize unwanted interactions of

the produced particles (nuclear interactions and coulomb scattering).

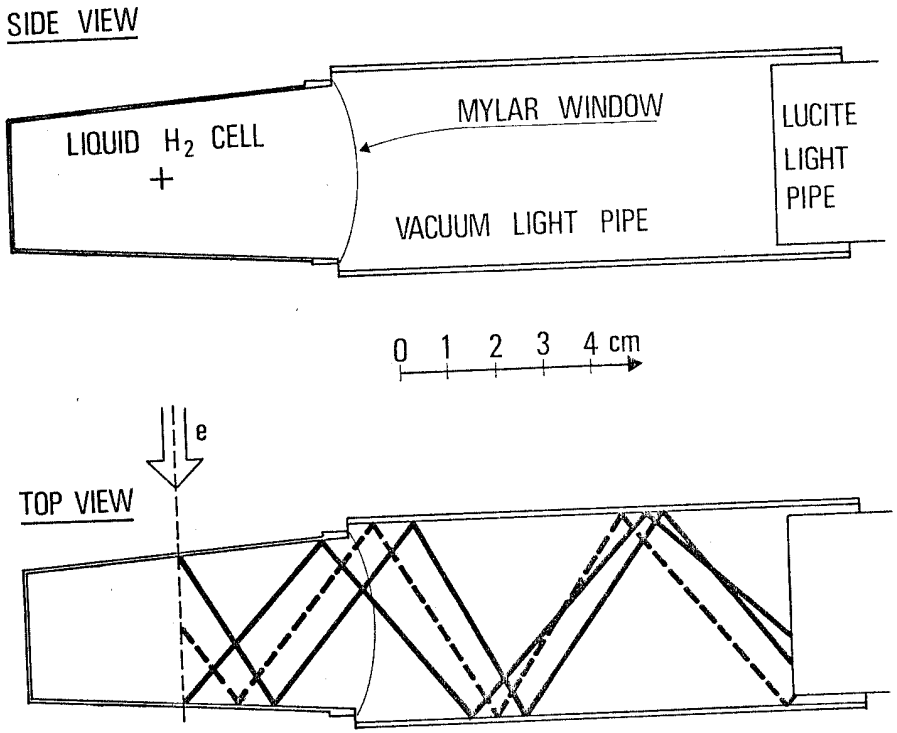

Fig. 4.2.36

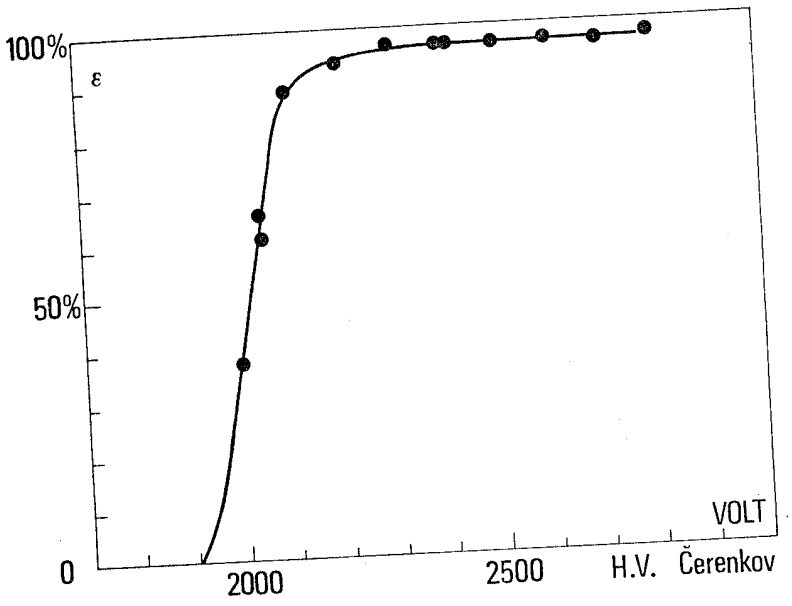

Fig. 4.2.37

Efficiency curve of the liquid H_2 Cerenkov counter as a function of the high voltage of the phototube. (11)

As far as the momentum region $p \gtrsim 2$ GeV/c is concerned gas Cerenkov counters with typical thickness of the order of 1 m, are needed. This means that such devices have to be located outside the magnetic volume (distance from the beam line of the order of 1 m) and that solid angles larger than 20% of 4π are hardly coverable. For instance, a request of a solid angle of $\sim$ 10% 4π means a gas Cerenkov whose front window

covers an area of the order of 4 m^2. Such large Cerenkov counters have been already built and successfully tested when using commercial gases such as $C_5 H_{12}$, Isobutan, Freon etc. at pressures up to 2 - 3 atm. A particular realization (10) of a large, wide aperture multi-cell Cerenkov detector (front window (2.5 x1) m^2, thickness 1.75 m) has been tested at SLAC (see Fig. 4.2.38) achieving a very good single-particle separation when used as a threshold counter.

In conclusion, a chain of three Cerenkov counters (liquid H_2, lucite and gas) allow the separation among π's and K's in the whole momentum range involved in the multihadron production at a Super Adone type machine. It is furthermore worth noticing that the pulse height analysis of these three Cerenkov counters may allow also a good K/p separation for momenta larger than 450 MeV/c (that is the Cerenkov threshold for K's in lucite). In connection with the protons selection, it can be recalled that always an antiproton is present when a proton is produced and that this fact may well be taken into proper account to fully exploit the advantages of the peculiar antiproton signature. The time of flight measurement also help when protons are present.

A last remark may be made on the convenience of complementing the series of the Cerenkov detectors with an hadronic filler, some interaction lenghts thick, which, even if in a limited solid angle, could perform a clear indentification of the μ's.

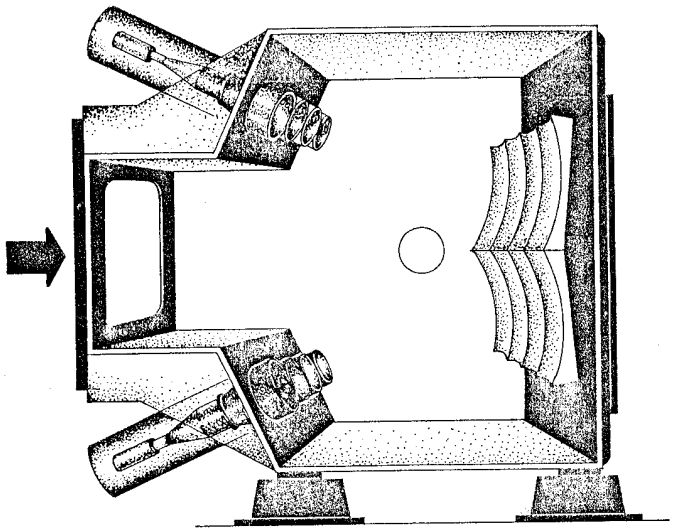

a)

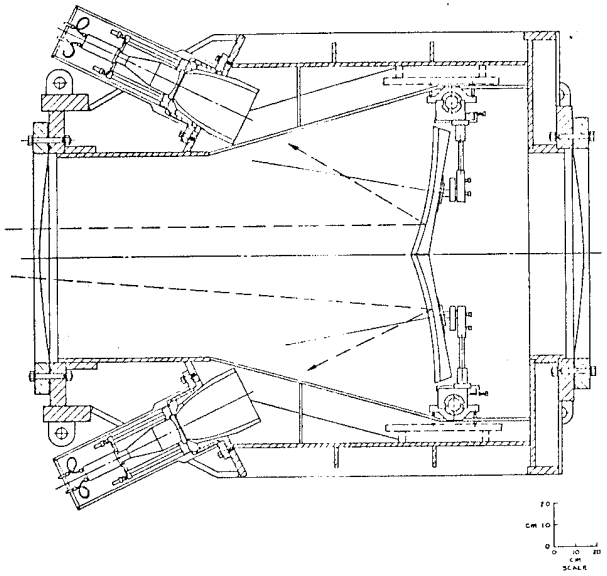

b)

Fig. 4.2.38

Large multi-cell Cerenkov detector (described in ref. 10)

4.2.5. Neutral detection

The detection of charged tracks only is clearly not sufficient to the proper evaluation of efficiencies in the reconstruction of the total hadronic annihilation cross section σ_T. Also, the precise individuation of the dominant hadronic channels and the determination of the average multiplicity are not possible without the detection of neutrals.

The problems of detecting γ's can be thought of at three different levels:

1) γ- counting, to assign the event it's peculiar topology.

2) Determination of the angless θ_γ and φ_γ of the γ with the beam line. In some cases this measurement allows a complete kinematic reconstruction of the event and might be enough to decide whether two γ's come from the same π° or η°.

3) Measurement of the γ energy to have a fully complete kinematic reconstruction.

The first two problems, counting and angle determination, necessarily need a solid angle as large as possible. This does not require much material and can be restricted to a reasonably thin shell around the interaction region.

However, the energy measurement needs much more space occupied by detectors and then a substantially larger cost.

It must be noted that, at least for what concerns the reconstruction of topologies, a missing γ in a γ- pair from π°,

η° can be tolerated thus softening a little the prescription on solid angles.

Counting and localization of γ's can be done by means of a sandwich consisting of alternate layers of MWPC and lead. The coordinates must be taken on many separate planes and the total lead thickness must guarantée a high efficiency. Each absorber, however, need be thin enough to allow:

a) a low detection threshold (this problem must be considered in connection with the thickness of the internal coil of the magnet);

b) determination of the conversion point with a reasonably small error.

The energy spectrum of γ rays from Π° decay in $e\bar{e} \to 8\Pi$ at 10 GeV has been estimated and clearly shows that even if most γ's have energies in the range 500-1000 MeV, the number of softer γ's is not negligible.

In general the pairing problem to reconstruct the Π° mass is non-ambiguos only for $2\Pi^0$ in the final state. With one more produced Π° some consistency test can be used based on the aperture angle of the 2 γ's (to get a rough indication on the energy) once a given pairing is assumed (see fig. 4.2.39).

The measurement of the energy can be obtained by adding to the part used for localization a further detector in which the shower can be totally absorbed.

We think of three different solutions already adopted in many experiments:

1) Lead-glass Cerenkov counters. The energy resolution is of the order

$$\frac{\Delta E_\gamma}{E_\gamma} \simeq \pm \frac{0.05}{\sqrt{E_{\gamma\,\mathrm{GeV}}}}$$

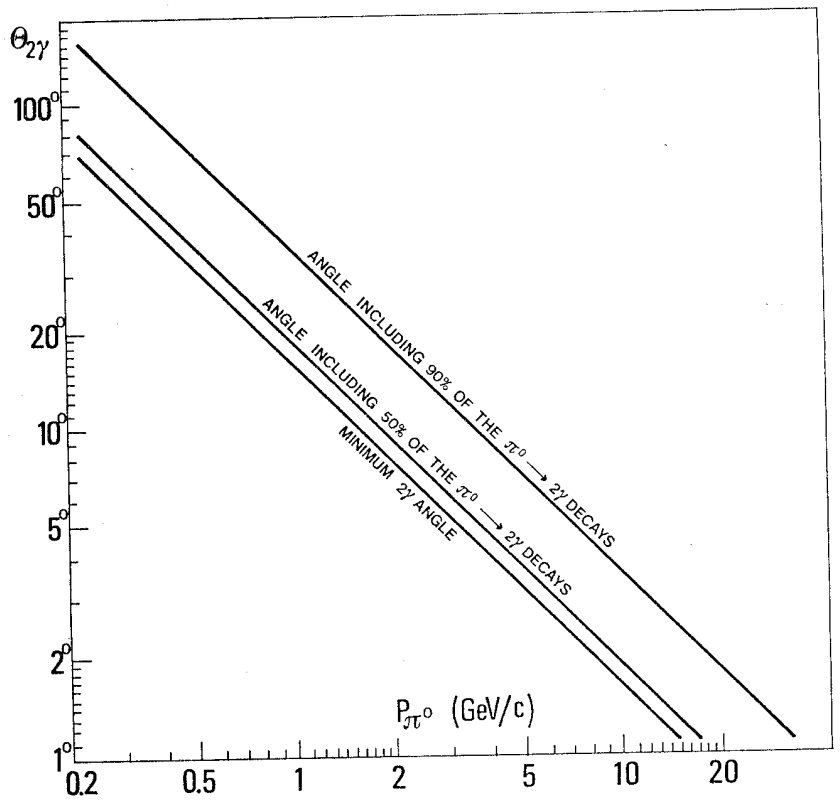

FIG. 4.2.39 -
2γ aperture angles in $\pi^\circ \to \gamma\gamma$ decay as a function of the π° momentum

2) Sodium Iodide scintil lation counters for which

$$\frac{\Delta E_\gamma}{E_\gamma} \cong \pm \frac{0.095}{\sqrt{E\gamma \text{ GeV}}}$$

3) Lead-Scintillation counters sandwich.

A choice among these possibilities is very much influenced by cost considerations. For Lead-glass Cerenkov counters it is in fact of the order of 50 ML/m^2; for Sodium Iodide it is up to 200 ML/m^2. In connection with a magnetic analyzer device, a γ detector with good energy resolution should be put outside the volume for momentum analysis and would hardly have a surface smaller than 40 m^2. Therefore, a practical tentative solution might consist in covering the whole surface with lead-MWPC sandwiches to get γ counting and localization. A smaller sector, perhaps 20% of the total solid angle, might be equiped with lead-glass Cerenkov counters to get energy determination on some of the γ-rays. This composite structure is analogous to the one proposed for Π/K separation.

This choice is not new and we show two different examples the multi-γ T.A.C. spectometer [12] (Fig. 4.2.40) and the Multi-γ apparatus at the ISR (CERN) (Fig. 4.2.41) [13].

An external γ detector for BEBC has also been recently proposed for the use at 400 GeV which uses a similar scheme [14].

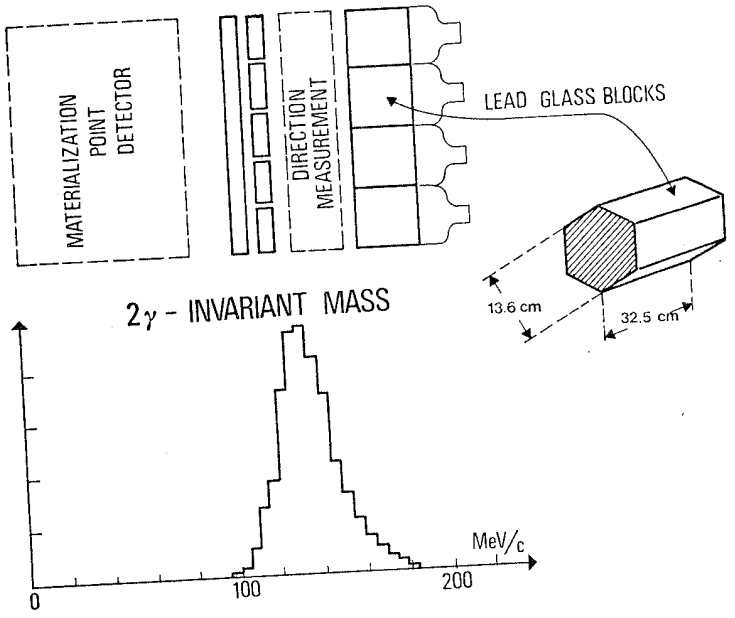

Fig. 4.2.40

A CERN multigamma spectrometer realization (Holder et al.) N.I.M. 108, 541 (1973)

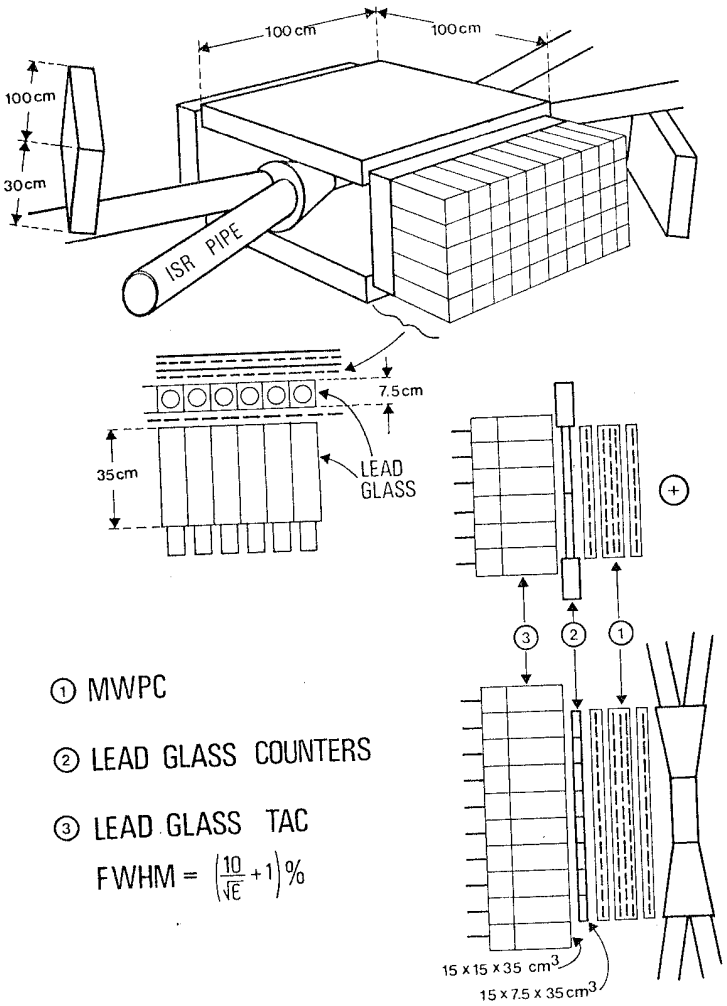

Fig. 4.2.41

In summary, we show in fig. 4.2.42 a possibile structure of a device suited for γ detection.

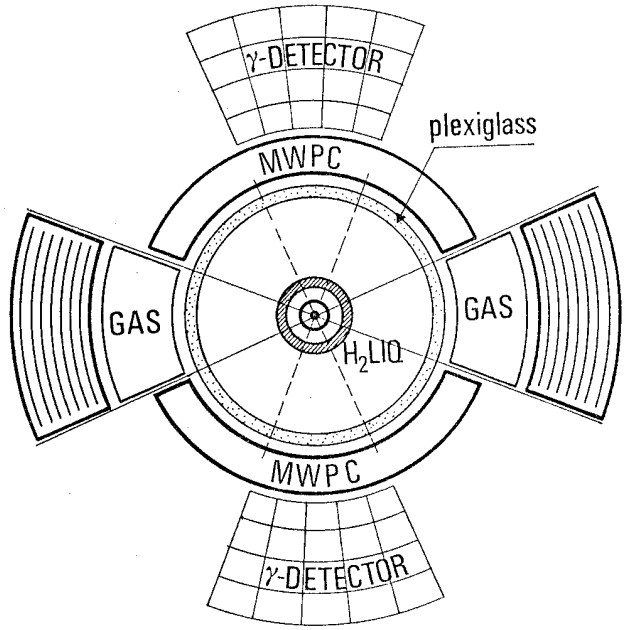

Fig. 4.2.42

We took into account the consideration already done concerning Π/K separation: therefore the core of the apparatus, fully cylindrical symmetric, is deserved to momentum analysis. The outside space is filled with plexiglas Cerenkov counters for Π/K separation up to 2 GeV and with a lead-MWPC sandwich system for γ counting and localization over a very large solid angle.

Eventually Π/K separation up to maximum energy and γ energy measurement is confined to smaller sectors covering 10% of the total solid angle each.

4.3 - Forward Electrons Tagging Systems

4.3.1. - Introduction

Recently, several theoretical works have shown the importance of two photon processes in e^+e^- (or e^-e^-) collisions in the energy region of some GeV [15], [16].

For example, the total cross section of hadronic two photon processes, $e\bar{e} \to e\bar{e}+X$ has been estimated by R. Gatto and G. Preparata [16] to be of the order of 10 - 15 nbarn. Almost 10nb of this are due to the production of resonances from two quasi-real photons and the rest of the cross section is calculated as due to a diffractive process where the two photons behave like hadronic particles. For inclusive production of hadrons in the process $e\bar{e} \to e\bar{e}+h+X$ even with a transverse momentum cut on p_t^2 of the order of 0.5 GeV^2, the cross section from two photon processes is larger than that of one photon annihilation for $s=4E^2 = 200\ GeV^2$ (Fig. 4.3.1.). Such a large cross section of two photon processes implies the possibility of investigation of almost real and perhaps also virtual $\gamma\gamma$ collisions using the existing or coming e^+e^- (or e^-e^-) colliding beam storage rings.

The processes $\gamma\gamma$ into hadrons are also of interest since they provide a tool to investigate the electromagnetic properties of the hadron currents. The large cross section of the two photon processes may turn out to be a serious background for the study of the one photon annihilation processes. A clear separation of the two phenomena requires the detection of the primary leptons, be

cause the measurement of the energy of the hadron state could suffer from geometrical inefficiency or from the escaping of energy in the form of undetectable neutral particles (K_L, neutrons).

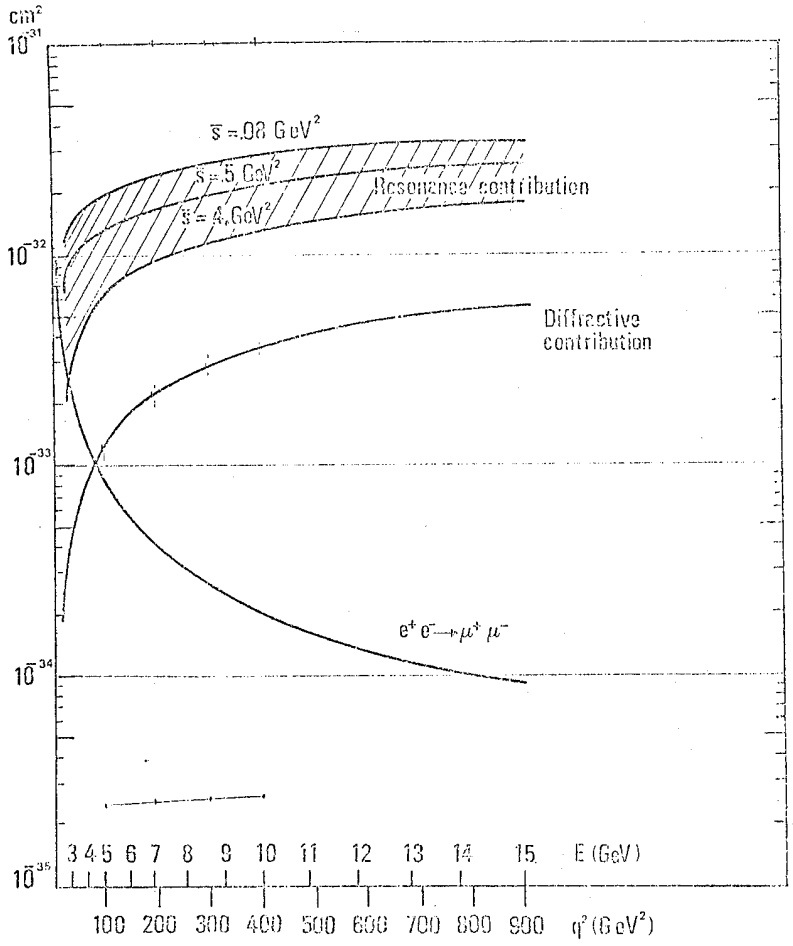

Fig. 4.3.1

The detection system for the forward emitted electron in the $e^+e^- \to e^+e^-X$ processes, (called the tagging system)has been successfully used in the magnetic structure of Adone [17,18]. The Adone tagging system has shown that the detection of the final electron with high efficiency in a large energy range is feasible, and that for the Adone experiment the contamination of two photon events in the annihilation channel was limited to a small percentage.

4.3.2. - The tagging system

The tagging system for a low β magnetic structure like that of Super-Adone has been studied in ref. (19) and is schematically shown in Fig. 4.3.2.

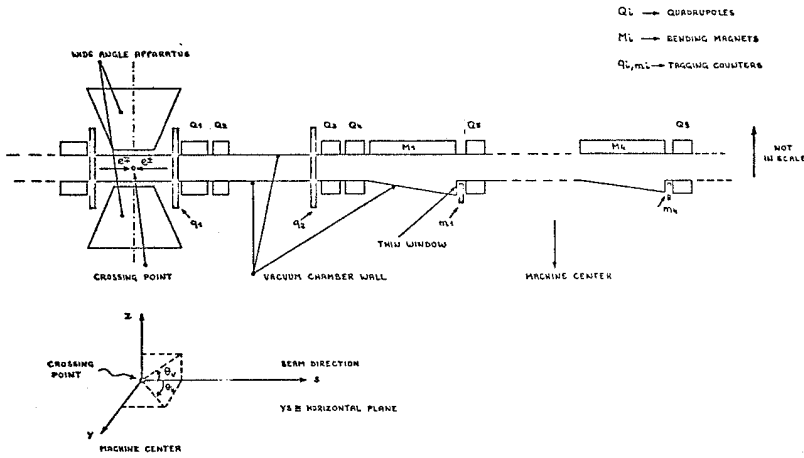

Fig. 4.3.2.

Counters q_1, q_2 and $m_1 \ldots m_4$ are all shower counters that will give information on the energy and the position of the electrons. q_1 and q_2 will have the best energy resolution since in $m_1 \ldots . m_4$ the energy information is given by the magnet and the measurement of the energy deposited in the counters will be essentially used to reject low energy background.

Angular and energy acceptance of the tagging system

The angular acceptance of q_1 is energy independent because the region from the interaction point to q_1 is free from magnetic field and its lower limit is determined by the vacuum chamber shape, which is assumed to be elliptical as shown in Fig. 4.3.3 and its upper limit by the q_1 dimension:

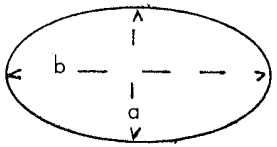

Fig. 4.3.3

If we take b = 15 cm and a=5cm the angular acceptance becomes:

$$\begin{cases} 42 \leq \theta_H \leq 100 \text{ mrad} \\ 14 \leq \theta_V \leq 100 \text{ mrad} \end{cases}$$

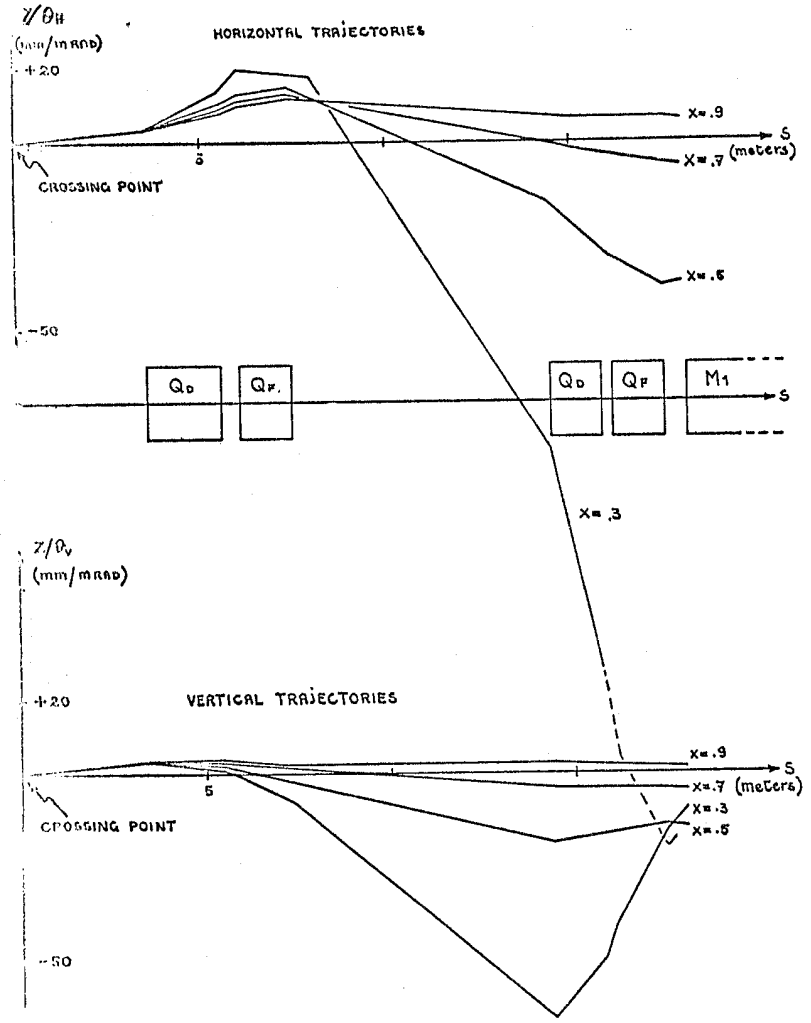

Fig. 4.3.4

The angular acceptance of q_2 is determined by the characteristics of the quadrupoles as shown in Fig. 4.3.4 and is a function of the fractional energy X. Its values for three typical X values are:

$X = 0,3$ $\quad \begin{cases} 1,8 \leq \theta_H \quad 7,5 \text{ mrad} \\ 0,8 \leq \theta_V \leq 6 \quad \text{mrad} \end{cases}$

$X = 0,5$ $\quad \begin{cases} 9 \leq \theta_H \quad 10 \text{ mrad} \\ 2,5 \leq \theta_V \leq 14 \text{ mrad} \end{cases}$

$X = 0,9$ $\quad \Delta\theta_H \simeq \Delta\theta_V \simeq 0$

The angular acceptance of counters $m_1 \ldots m_4$ is shown in Fig. 4.3.5 as a function of the fractional energy X. The acceptances are derived from Fig. 4.3.4 requiring that the electron reaches the first dipole without crossing the vacuum chamber wall. Fig. 4.3.6 (a) shows the intersection points of a particle trajectory, defined by the initial angle θ_H and the fractional energy X, with a vertical surface Σ parallel to the beam trajectory at a distance y = 15 cm in the direction of the machine center. The surface Σ is the border between the magnetic and the free field region. The lines for $|\theta_H| > 0$ are limited at the lower X values by the magnet gap as already shown in Fig. 4.3.5. In Fig 4.3.6(b) the angle θ_H^{out} of the electrons with the surface Σ is shown. From this figure we see that the Super-Adone vacuum chamber has to be of particular shape in the tagging region of m_i in order to minimize the material to be crossed by the tagged electrons.

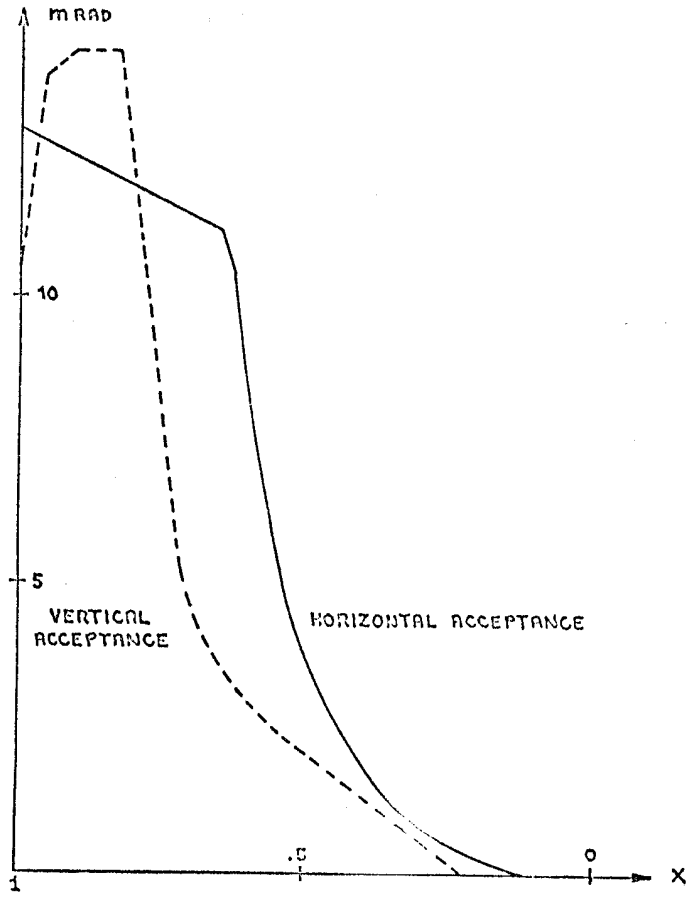

Fig. 4.3.5

The angular acceptance of q_2 is determined by the characteristics of the quadrupoles as shown in Fig. 4.3.4 and is a function of the fractional energy X. Its values for three typical X values are:

$X = 0,3$ $\quad \begin{cases} 1,8 \leq \theta_H \quad\quad 7,5 \text{ mrad} \\ 0,8 \leq \theta_V \leq 6 \quad \text{mrad} \end{cases}$

$X = 0,5$ $\quad \begin{cases} 9 \leq \theta_H \quad\quad 10 \text{ mrad} \\ 2,5 \leq \theta_V \leq 14 \text{ mrad} \end{cases}$

$X = 0,9$ $\quad \Delta\theta_H \simeq \Delta\theta_V \simeq 0$

The angular acceptance of counters $m_1 \ldots m_4$ is shown in Fig. 4.3.5 as a function of the fractional energy X. The acceptances are derived from Fig. 4.3.4 requiring that the electron reaches the first dipole without crossing the vacuum chamber wall. Fig. 4.3.6 (a) shows the intersection points of a particle trajectory, defined by the initial angle θ_H and the fractional energy X, with a vertical surface Σ parallel to the beam trajectory at a distance y = 15 cm in the direction of the machine center. The surface Σ is the border between the magnetic and the free field region. The lines for $|\theta_H| > 0$ are limited at the lower X values by the magnet gap as already shown in Fig. 4.3.5. In Fig 4.3.6(b) the angle θ_H^{out} of the electrons with the surface Σ is shown. From this figure we see that the Super-Adone vacuum chamber has to be of particular shape in the tagging region of m_i in order to minimize the material to be crossed by the tagged electrons.

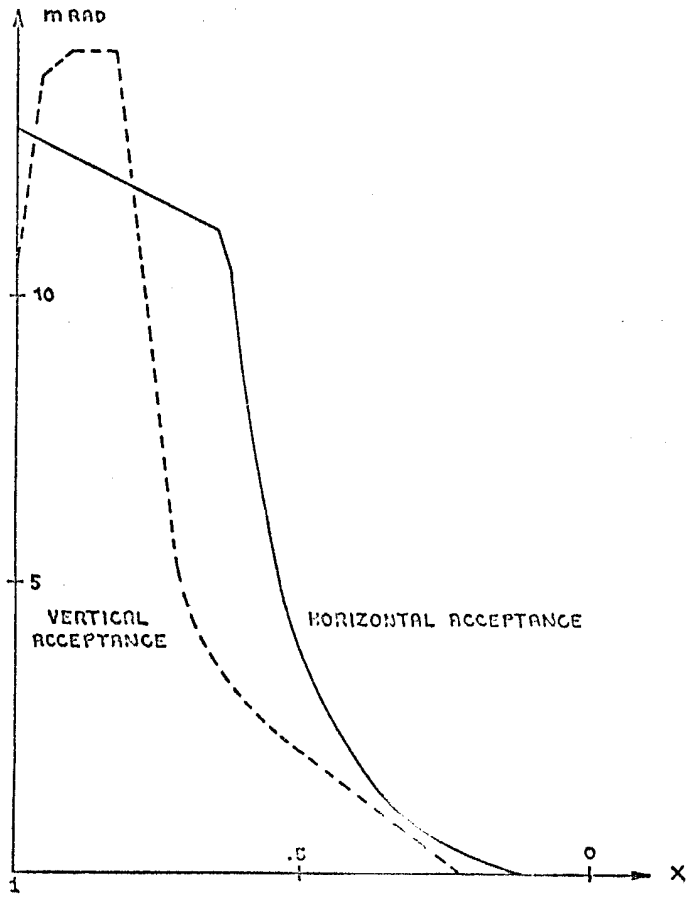

Fig. 4.3.5

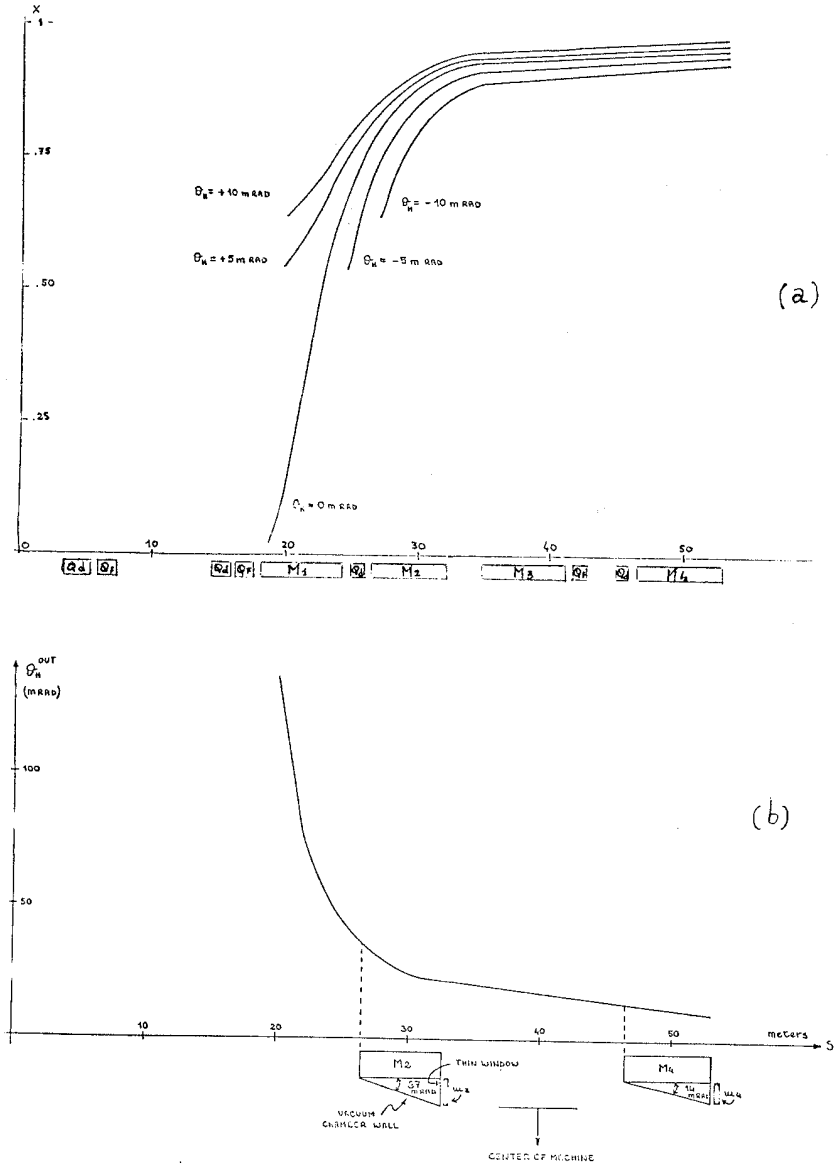

Fig. 4.3.6

Background of the tagging counter

The most serious background in the tagging counters is caused ty the electrons which have lost energy in beam-beam and beam-gas bremsstrahlung. Even though beam--gas bremsstrahlung may be neglected due to the ultrahigh vacuum existing inside the chamber, because of the high luminosity foreseen for Super-Adone, in the one bunch operation ($L = 10^{32} cm^2$ sec $^{-1}$) beam-beam bremsstrahlung will cause the tagging counter to be hit by 50 e^- or e^+ per bunch-bunch interaction with $X \geq 5\ 10^{-2}$. These electrons will simulate tagging events in the tagging counters.

A very promising solution to this serious problem has been proposed, namely to on distinguish on a statistical basis the bremsstrahlung electrons and the electrons from two photon processes from their different angular distributions[20]. As shown in Fig. 4.3.7 the angular distribution of the electron bremsstrahlung is characterized by an angle of the order of m_e/E. In the two photon processes the electron emission angle is of the order of $\sqrt{m_e/E}$. If the angular acceptance of the tagging system is properly chosen most of the bremsstrahlung electrons can be rejected with a small loss of two photon electrons. Table IX gives the preliminary results obtained for the relative acceptances of the electrons coming from bremsstrahlung events A_b or from photon-photon events $A_{\gamma\gamma}$, for electrons having an energy X =0,95. The angular spread of the primary beam has been taken into account assuming

$\sigma_{\theta_H} = \sigma_{\theta_V}$ =0,7 mrad

TABLE IX

	$\theta_c = 0$	$\theta_c = 1$	$\theta_c = 1.5$	$\theta_c = 2$
$A_{bremss.}$	1	0.15	$3\ 10^{-2}$	$4\ 10^{-3}$
$A\ \gamma\gamma$	1	0.37	0.29	0.25

θ_c in mrad gives the lower limit of the emission angle accepted by the tagging counters: as shown by the table it is possible to have a rejection 2 orders of magnitude on bremsstrahlung events with a reasonable loss of $\gamma\ \gamma$ events. If both tagging counters are required in a trigger the acceptance A_{bremss} and $A\ \gamma\gamma$ have to be squared.

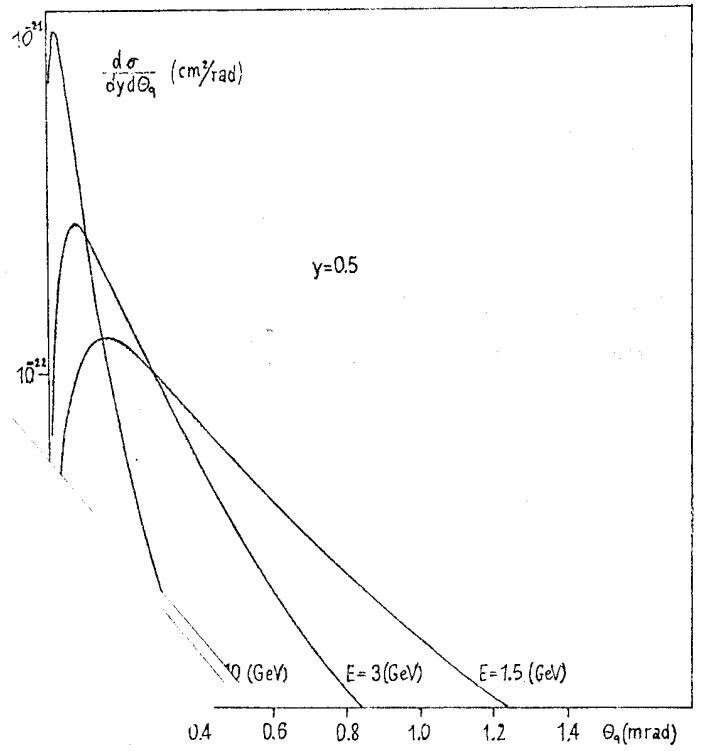

pa
mir
tror

Another solution to the problem of accidental coincidences due to the bremsstrahlung electrons has been proposed by several authors who suggest a multi-bunches ring, in order for the accidentals per bunch to be kept at a reasonable level while still attaining comparable total luminosity.

4.3.3. - The wide angle apparatus. (W.A.A.)

The two photon processes also have the following relevant features in which they differ from the one photon annihilation:

i) the frame of the reference of the two photons is in general moving along the beam direction, so that the angular distribution of the final state is forward peaked around the electron or positron direction; with an angular distribution that can be easily measured by the W.A.A. as shown in figures 4.3.8, 4.3.9.

ii) the equivalent photon energy spectrum[15]

$$N(\omega) = \frac{2\alpha}{\pi} \frac{1}{\omega} \ln \frac{E}{m_e}$$

contains many low energy photons and the total energy of the state produced by the $\gamma\ \gamma$ interaction is usually much lower than the total available energy 2 E.

In order to use the above features, the wide angle apparatus that will detect the $\gamma\gamma$ events must measure the particle energy and it must cover the smallest possible angle in the forward region. An example of a magnetic detector especially suited for detecting $\gamma\gamma$ events is the magnetic apparatus proposed for the investigation of this

process at VEPP 4, the 7 GeV Novosibirsk e^+e storage ring[21].

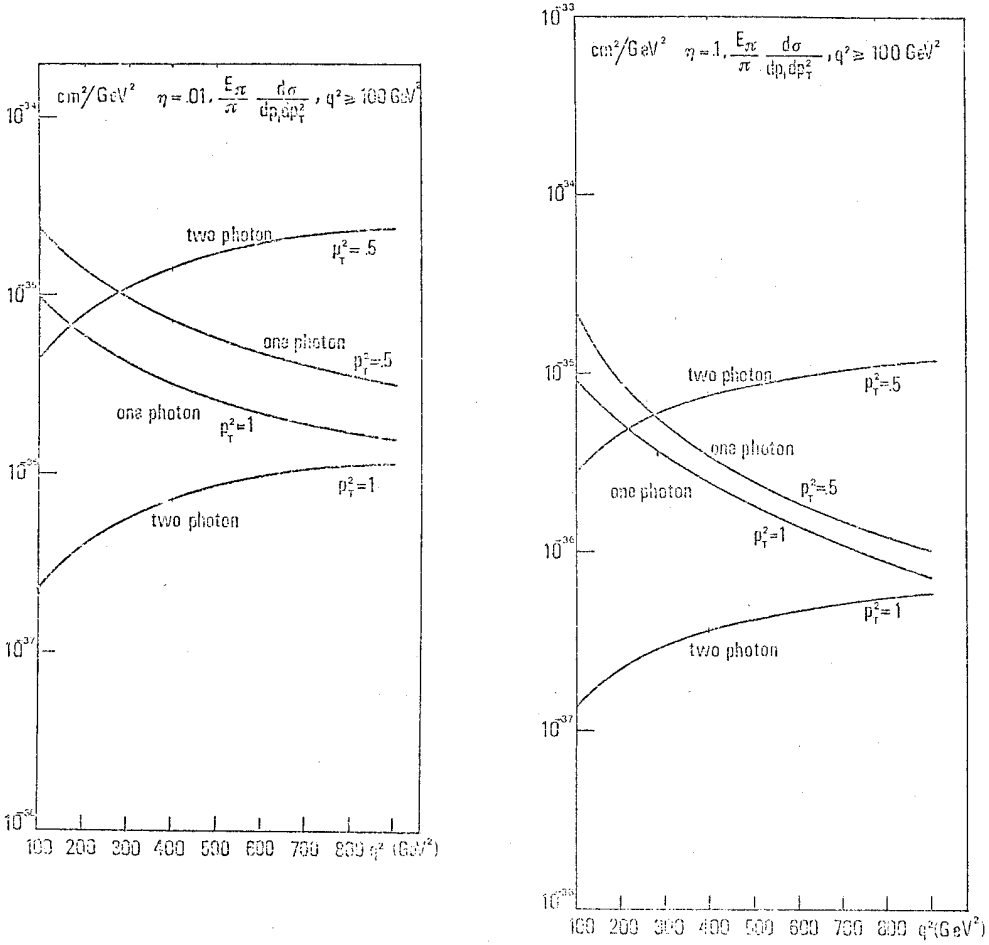

Fig. 4.3.8

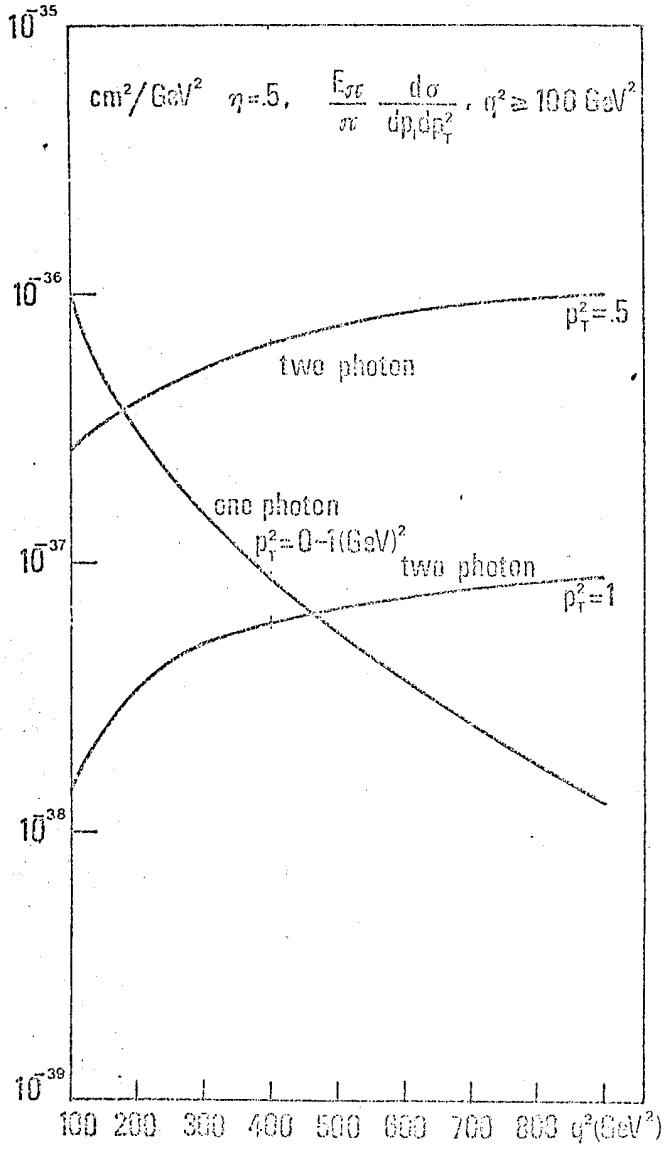

Fig. 4.3.9

The magnetic field of the storage ring bends the interacting lepton pair towards the inside of the magnet. Thus that portion of the magnetic path adjacent to the region of collision must be designed so as to allow for the detection of the particles of interest and their energy analysis. This is schematically shown in Fig. 4.3.10.

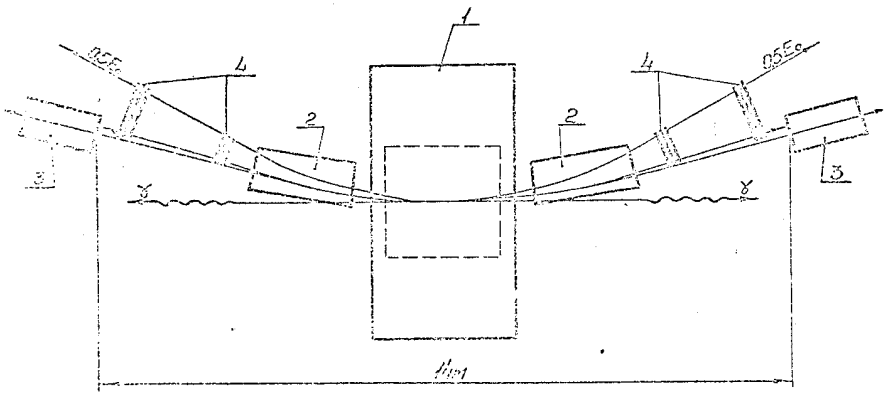

Fig. 4.3.10

Another wide angle apparatus suitable for the $\gamma\gamma$ investigation could be the total solid angle array of a total absorption calorimetric spectrometer, recently proposed for inclusive experiments at the ISR[22] (Fig. 4.3.11).

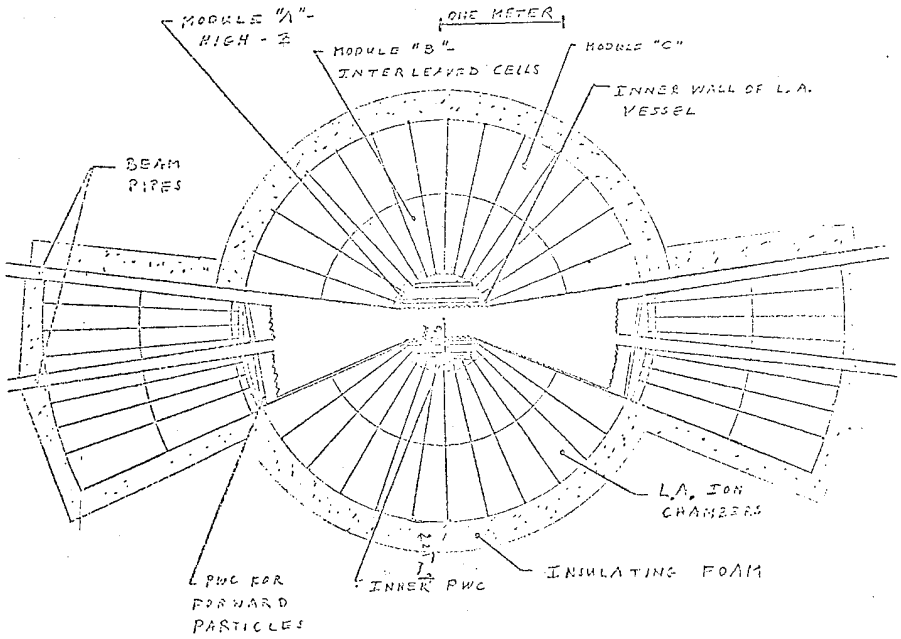

Fig. 4.3.11

The most interesting property of this apparatus for the $\gamma\gamma$ interaction is that the calorimetric part of the spectrometer can efficiently cover the forward region. In this apparatus one could investigate the diffractive part of the $e\bar{e} \rightarrow e\bar{e}$ X cross section at the studied for the ISR highest energies. This proposal, however, needs further study to be considered as an experimental apparatus for $e^+ e^-$ storage rings.

4.4. Data Acquisition

Introduction

Future experiments with high energy electron-positron storage rings will probably make extensive use of multiwire proportional chambers (MPWC), because of the attractive features of high acquisition rate, resolution and multitrack efficiency of such detectors.

On the other hand the increase in the acquisition rate corresponds to an increase in the data processing speed requirements, which could approach the maximum possibilities of the biggest available computers. An example showing the importance of this problem is given by the CERN-ISR Split Field Magnet, in which 10^5 events/sec. take place, 10^3 of which are interesting, while the CDC 7600 on-line system is only capable to analyse 1 event/sec. Fortunately the expected rates on the electron-positron storage rings are lower than the I.S.R. rates, but the data acquisition and processing power of the Laboratory is still one of the problems to be taken into careful consideration.

The use of a central big computer on-line with the experiments should be avoided as far as possible because it is expensive and it interferes with the other uses of the centre. For this reason we will later suggest the introduction of a new kind of hardware processor to be coupled to some experiments, which could improve the data processing speed, thus allowing a reduction in the power and cost of the central computing system.

Computer network

As each experiment will probably use a small computer in its data acquisition system, a standardization of these small systems is convenient. This should not be limited to the interfacing electronics, where the worldwide accepted standard is now CAMAC, but could also be extended to the small computer systems. In this way a few specialists could provide a very useful general facility in the form of assistance to the experimental teams for both hardware links and software problems, which could thus be solved in a standard and modular way. They could also provide the maintenance of the data link between these remote computers and the central computer. This link would make available to each experiment all the computing power of the big computer and in particular:

- the floating point computing speed;
- the high level programming languages;
- the extended programme library;
- the direct storage into permanent files on magnetic tapes and disks of the central computer, thus avoiding tape transport problems.

The increase in the central computer core dimensions needed for this link, can be compensated by a reduction in the dimensions of the remote small computers and by the improvement of the central computer system facility.

The computer network will have the configuration shown in Fig. 4.4.1.

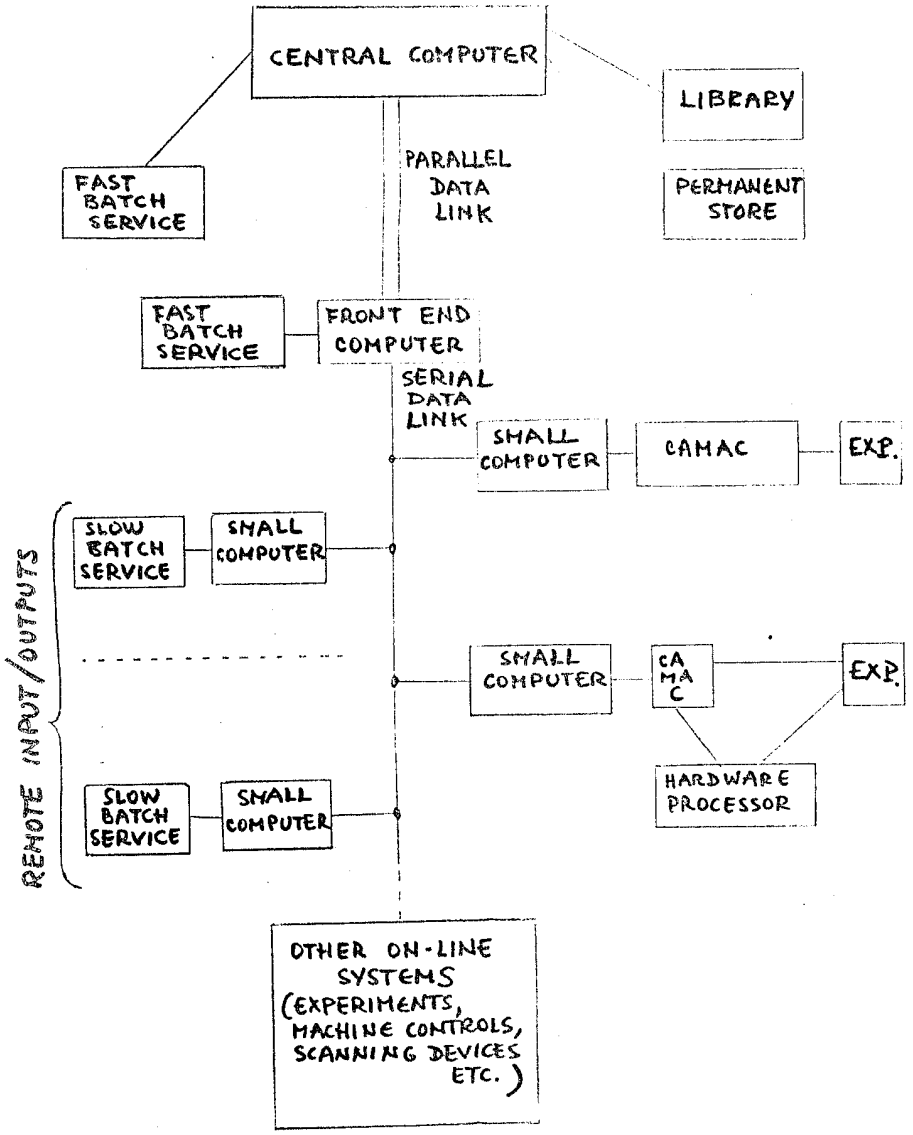

FIG. 4.4.1 - Computer Network Configuration

A front-end computer will manage the link with all remote small computers which will accomplish the following functions:

- interrupt handling;
- data acquisition and temporary storage;
- external parameter control;
- fixed point and simple floating point calculations;
- output and display of the results.

The on-line central computer facility will be tipically used for:

- complete analysis of data samples to check and monitor the experiments;
- production of sophisticated outputs and displays;
- direct storage on permanent data files in the central computer;
- possible complex on-line floating point calculations.

The data link with the central computer will also allow a few remote input/outputs to be placed around the centre for directly submitting (in the self-service mode and under system control) user jobs to the central processor.

The typical small computer could have a 8K 16- bit word core, while the central computer size will depend on the number of users and their requirements.

In the proposed scheme the possibility of high data transfer rates between the experiments and the central computer is not foreseen. In fact this would not be an efficient use of the

data link, it would interfere with the other users and would result in a higher cost of the experiment. For this reason we suggest to implement the experiments needing high on-line computing speed (whenever possible) with fast hardware data processing systems.

An example of utilization of such systems is also included in fig. 4.4.1.

This hardware processing can be made essentially in three ways: analog, digital boolean and digital arithmetic.

The analog way consists in building an analog device for the particular problem to be solved and in inserting it in between the apparatus and the computer to get a fast data preselection and reduction.

Another way consists in storing the MPWC pattern of fired wires, for instance, in a series of shift registers. This allows a recursive check with the same boolean functions to be carried out on the complete data pattern (23).

The third method is practicable when the event identification is based on numerical calculations made on the rough digital data collected by the apparatus. This is normally possible with the MPWC as the address of the fired wires are available in digital form.

Fast hardware processors

A method to increase the data processing speed is to use a parallel instead of a serial logic, the latter being used

in conventional computers. Nevertheless such a method has many inconveniences such as the electronic complexity and the reduced versatility due to the loss in the ability to programme the system. In fact in some laboratories some special-purpose fast hardware processors have been built to solve the problems faced in analysing MPWC's data (24).

To allow a more general and easy use of these hardware processors we propose to introduce a modular system which has not only the advantages of the systems using the parallel logic, but also a certain possibility to be programmed. This would allow one to build special purpose data processing systems as a sequence of elementary modules, as in a computer one makes a program as a sequence of elementary instructions.

This modularity is very important because it allows one to build and change very easily the hardware program which is executed without any electronic engineering.

The system will be formed by one or more crates, with a number of common lines, in which the electronic cards, each one corresponding to a module, are placed. A simple example of a modular system is shown in fig. 4.4.2: A, B,C and D are fixed digital parameters; the input of x into the system will start the sequence of the add and multiply operations indicated so that at the end the digital number corresponding to the polynomial $AX^3 + BX^3 + CX + D$ will result on the output.

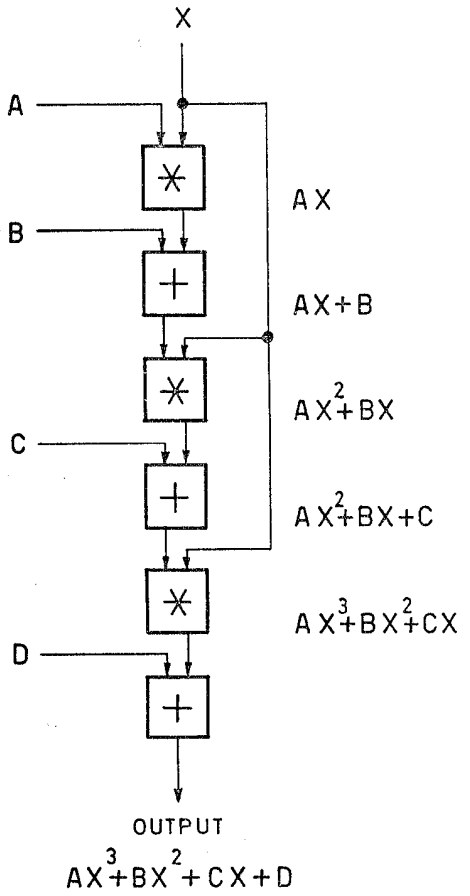

FIG. 4.4.2

Example of polinomial calculation

This hardware execution of the calculation can require a time up to two orders of magnitude shorter than in the small computers.

The calculation just described is actually a serial operation; an important feature of the hardware modular system described, which is not found in small computers, is the possibility of parallel operation, which contributes to an increase in speed.

Before going into some details of the operation of the modular system, we show another example to clarify how these serial and parallel operations can work: in fig. 4.4.3 one can see the sequence of modules required to compute the triple integral:

$$\int_{XMIN}^{XMIN+DX} dx \int_{YMIN}^{YMIN+DY} dy \int_{ZMIN}^{ZMIN+DZ} F(x,y,z)\,dz$$

The function F(x,y,z) can be made by either a sequence of elementary digital modules similar to that shown in fig. 4.4.2 or by a mixing of digital and analog modules, which allows fast and approximate calculations of complex functions.

The modules indicated by X_i and P_i are two coupled read only memories (ROM) which contain, for instance, the 24 points and the 24 weights for the gaussian quadrature (fixed parameters).

At each "clock" pulse (see fig. 4.4.3) the read only memories shift by one position presenting on the output both the

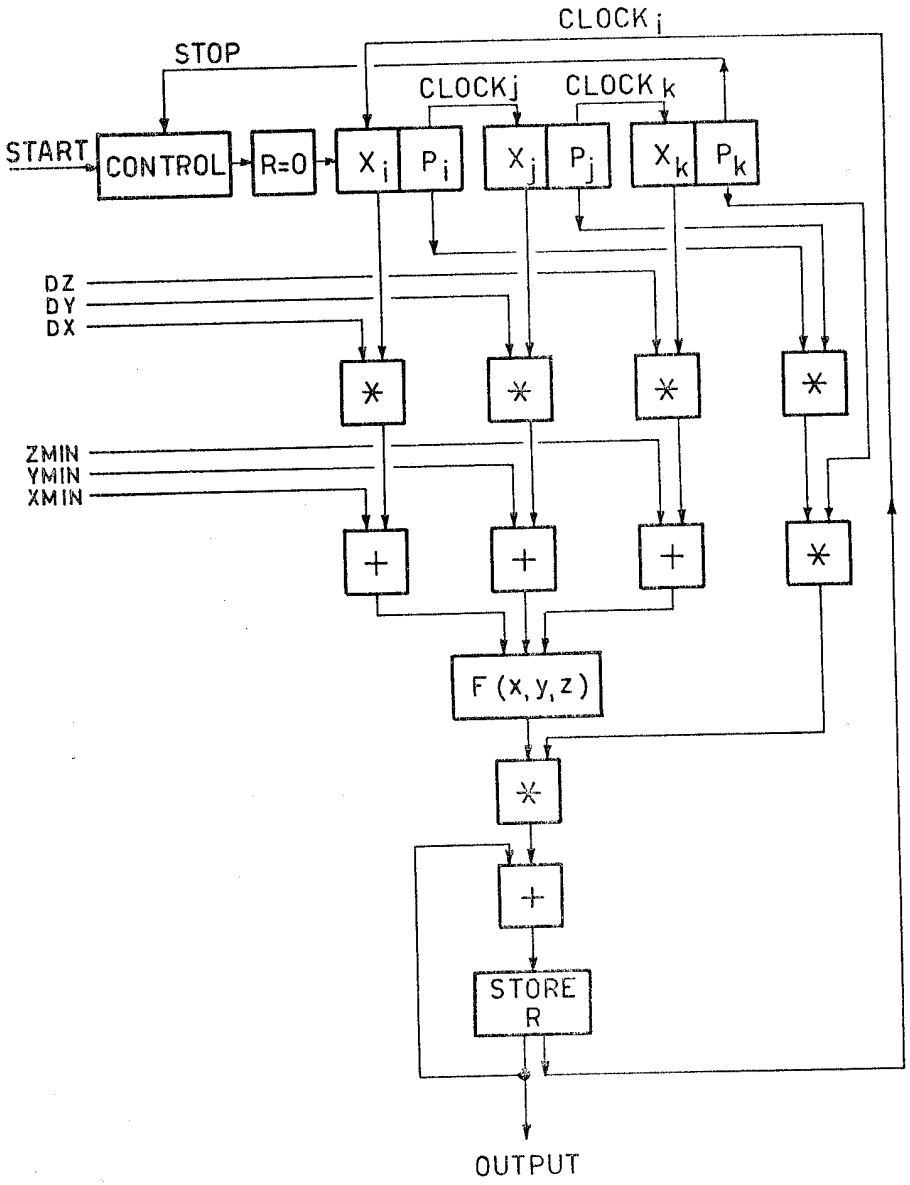

FIG. 4.4.3 - Hardware system computing a triple integral e.g. by gaussian quadrature.

next point X_i and weight P_i (as digital numbers). After 24 "clock i" pulses the next pulse will arrive also to the second couple of ROM (X_j and P_j) as "clock j" (see fig. 4.4.3). In this way every 24 "clock i" pulses one "clock j" pulse is sent to the second store (X_j,P_j) and similarly every 24x24 "clock i" pulses one "clock k" pulse is sent to the third store (X_k,P_k). This is equivalent to a triple loop in which the actual calculations are carried out 24x24x24 times within the hardware processor without any input/output requirements, which would slow down the speed.

The equivalent Fortran programme would be:

```
      R=0
      DO 1  I=1,24
      XX=XMIN + DX * X(I)
      DO 1    J=1,24
      YY=YMIN + DY * Y(J)
      DO 1    K=1,24
      ZZ=ZMIN + DZ * Z(K)
    1 R=R + P(I) * P(J) * P(K) * F(XX,YY,ZZ)
```

In this example one clearly sees how parallel calculation can be carried out: all the operations corresponding to boxes on the same horizontal line in fig.4.4.3 are executed at the same time.

We can also understand better now how the system would work to allow closed loop serial operation. In order to accomplish its function each module should wait until the previous modules have completed their operations, and

then, after an internal delay, not shorter than the time required to present to the output the result of its operation it should send a signal to the following module to which it is connected.

The connections of these lines determine the time sequence of the instructions ("program flow") corresponding to the modules.

In addition to this network which defines the program there must be other connections ("data lines") between the modules which generate and those which use these data.

The number of elementary modules can be quite limited and one could also introduce special purpose and analog modules (as A/D, D/A converters, scalers, analog function generators, amplitude to frequency converters, teletype divers, etc.).

The elementary functions needed are very similar to those we find in ordinary computers (jump, skip under condition, add, or, store, etc.).

Beside the obvious arithmetic and boolean function modules and the store module used to make the loops in Fig.4.4.3 we can mention a module capable of comparing two numbers A and B. This would give the "programm flow" signal on one of three independent outputs according to what condition is verified: A< B, A=B or A > B; this module will allow one to perform a "conditional skip". The "jump" is just made as a connection on the programm flow line. The "store" of the data is just one latch opened by the "program flow" signal.

It is worthnoting that in this system many modules behave like a register which stores its output data until its next cycle, so that the use of store registers is much less important than in the usual processors, in which partial results must be temporarily stored before being used again for futher calculations.

Finally the system control can be achieved by one control card containing two flip-flops (FLAG and CONTROL), which both the external device and each module can reach through the common lines of the crate. The FLAG will enable the "program flow": it will be set by the external start; when cleared, the "program flow" will stop (for instance when the output data must be sent to a slower device, like a computer).

The CONTROL will allow the system to send an interrupt to the external device.

An example of a hardware system which must compute and send to a computer two numbers R and S is shown in fig. 4.4.4. .A start signal from the computer sets the FLAG and clears the CONTROL flip-flops to start the "program flow".Before computing the number R, the register S is cleared because both R and S are read by the computer on the same data line after an OR circuit. When the result of the R calculations is present at the OR output a "set CONTROL" is done by an appropriate module to produce an interrupt on the computer which starts the acquisition of R. In the meantime the system proceeds with the calculation of S after which a "clear FLAG" module stops the "program flow" and waits for the computer to complete the acquisition of R. When the computer starts again the "program flow" with a "set FLAG" and "clear CONTROL", the re-

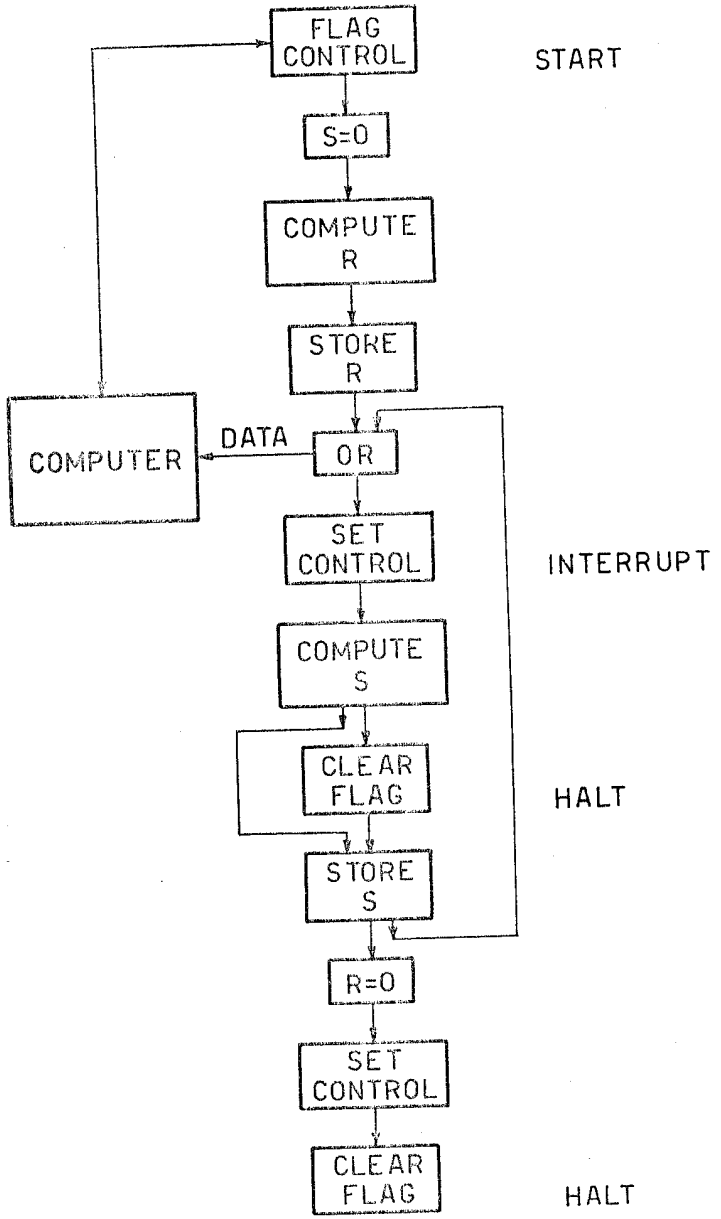

FIG. 4.4.4. - Example of the I/O system control

sult of the S calculation is stored on the register S and the register R is cleared so that on the output of the OR the number S is present. Then a "set CONTROL" module give another interrupt, which starts the acquisition of S by the computer, and a "clear FLAG" module stops the "program flow".

From this example it is apparent how the system input/output is controlled by a few control modules introduced in the system, in the same way as the equivalent instructions are used in a similar program of a computer.

The advantage of the hardware system is its speed which can be two orders of magnitude higher than in the small computers due to the microcircuits speed and the parallel operation.

In our opinion this modularity of the system is a big improvement which allows for cost reduction and simplicity in the building up and modifications of hardware systems.

A device along the lines described here is now under development in the Physics Laboratories of the Istituto Superiore di Sanità.

This work is a part of the research programme within the framework of the activity of the Sezione Sanità of the INFN.

REFERENCES TO CHAPTER 4

(1) W.Ash et al. - A magnetic analyzer to be used for Adone colliding beam experiments. Frascati Internal Report, LNF-69/2 (1969)

(2) A.Minten (Ed.) The split-Field Magnet facility, CERN-SFEM Note - S/Rev. October 1972
J.Billan, R. Perin, V.Sergo - The Split Field Magnet of the CERN - ISR - CERN - ISR-MA/72-53.

(3) A.Michelini "Spectrometers for High Energy Physics", proceeding of the "1973 International Conference on Instrumentation for High Energy Physics" Frascati (1973), pag. 633

(4) K.Steffen "Plans for the Storage Ring and Detection Apparatus at DESY" - DESY Internal Report DESY 70/24 (1970)

(5) H. Hultsching et al. " Ein magnetisher Detektor fur DORIS" DESY Internal Report

(6) W.Bartel et al. "Vorschlang für line Experimentieranordung bei der DESY - Speicherringen" - DESY Internal Report

(7) H.J.Besch, U.Trinks "Vorschlang für linen magnetishen Detekto am DESY-Speicherring" - DESY Internal Report

(8) E.Bertolucci, I.Mannelli, F.Martorana, G.Pierazzini, A.Scriba F.Sergiampietri and M.Vincelli. "Nucl.Instr.and Meth." 69,21 (1969)

(9) F.Sergiampietri- "Use of Cerenkov ligh in liquid H_2 targets". "Proc. of 1973 International Conference on Instrumentation fo High Energy Physics". Frascati, May 1973, pag. 430.

(10) H.H.Williams, A.Kilert and D.W. Leith SLAC-PUB 1070 - July 19

(11) P. Spillantini - Frascati Internal Report, LNF-74/6 (P), Submitted to Nucl. Inst. and Mith

(12) M. Holder, C. Padermacher, A. Stande, P. Darriulat, J. Deutsch, J. Pelcher, C. Rubbia, K. Tittel, C. Grosso Pilcher, M. Scirè, A. Villari: "A high resolution total absorption spectrometer for simultaneous detection of several high-energy γ-rays" Nucl. Instr. and Meth. 54, 108 (1973).

(13) C.L. Yuan, A. Uto, E. Amaldi, M. Beneventano, B. Borgia, P. Pistilli, J.P. Dooker: "Proposal for an experiment on the multigamma production at the CERN ISR" CERN/ISRC/72/22.

(14) NAPOLI-PADOVA-ROMA-FRASCATI-TRIESTE Collaboration: "An external gamma ray detector to be used with BEBC with the TST for experiments at the SPS" See also: ECFA 300 GeV Working Group Report vol. I,p.24.

(15) P. Kessler, Int. Colloquium on Photon-Photon Collision in Electron-Positron Storage Ring, College de France, Sept. 3-4, (1973).

(16) R. Gatto, G. Preparata, INFN Sez. Roma Nota Interna 479 (1973).

(17) G. Barbiellini, S. Orito, T. Tsuru, R. Visentin, F. Ceradini, M.Conversi, S.d'Angelo, M.L.Ferrer, L.Paoluzi and R.Santonico, Phys.Rev. Letters, 32, 385 (1974).

G. Barbiellini, F.Ceradini, M.L.Ferrer, S.Orito, L.Paoluzi, R.Santonico and T. Tsuru, LNF/74-10,1974

G. Barbiellini and S. Orito, Frascati LNF 71/17, 1971

(18) C. Bacci, R.Baldini Celio, G.Capon, R.Del Fabbro, C.Mencuccini, G.P.Murtas, G.Penso, G.Salvini, M.Spinetti, B. Stella and A.Zallo, Lett. Nuovo Cimento, 3 , 709 (1972)

(19) G.Vignola, B. Stella (unpublished, presented at Study week for the Super Adone project (1973)).

(20) G.Altarelli and B.Stella, Lett. Nuovo Cimento 9 (1974).

(21) V.A.Sidorov, Invited Talk at the Int. Colloquium on Photon-Photon Collisions in Electron Positron Storage Rings, Collège de France, Sept. 3-4 (1973).

(22) W.J.Willis, CERN/ISRC/71-1.

(23) P.Waloshek et al - Proceedings of the International Conference on Instrumentation for High Energy Physics. Frascati 8-12 May 1973 page 287

(24) See for instance: M.Hansroul, C.Verkerk and P.Zanella - "Hardware Processors for Pattern Recognition Tasks in Wire Chamber Data", presented at the International Conference on Instrumentation for High Energy Physics. Frascati 8-12 May 1973.

A.A.Derevshchikov et al - "Fast Digital Processor for Applications in High Energy Physical Experiments" Nuclear Instruments and Methods 108, 381 (1973).

M. Schmit, J. Herry and Y. Flamant - "Operateur arithmetique cablé pour identification de particules" Nuclear Instruments and Methods 91, 321 (1971).

5 - Theoretical considerations

5.1 - R.Gatto: Some Problems and Perspective for e^+e^- Colliding Beam Physics.

5.2 - G.Altarelli, L.Maiani: Charmed Particles and Heavy Leptons

5.3 - A.Bramon, E.Etim, S.Ferrara, M.Greco, A.F.Grillo, G.C.Rossi Y.Srivastava: Theoretical Aspect of High Energy Electron--Positron Collisions.
1) e^+e^- annihilation and E.V.D.M.
2) Sum Rules in inclusive e^+e^- annihilation.
3) Gribov-Lipatov relation and connection between deep-inelastic scattering and annihilation.
4) Multiplicities and multiparticle production in an independent emission model for e^+e^- annihilation.

5.4 - R.Gatto, G.Preparata: Theoretical Studies for Higher Energy e^+e^- Collisions.

5.5 - P.Gensini: Aspects of Hadon Pair Production in e^+e^- Colliding Beams at High Energies.